Intervehicle Communication: Cox-Fox Modeling

Youngmin Jeong, *Student Member, IEEE*, Jo Woon Chong, *Member, IEEE*, Hyundong Shin, *Senior Member, IEEE*, and Moe Z. Win, *Fellow, IEEE*

***Abstract*—Safety message dissemination in a vehicular ad-hoc network (VANET) requires vehicle-to-vehicle (V2V) communication with low latency and high reliability. The dynamics of vehicle passing and queueing as well as high mobility create distinctive propagation characteristics of wireless medium and inevitable uncertainty in space-time patterns of the vehicle density on a road. It is therefore of great importance to account for random vehicle locations in V2V communication. In this paper, we characterize intervehicle communication in a random field of vehicles, where a beacon or head vehicle (transmitter) broadcasts safety or warning messages to neighboring client vehicles (receivers) randomly located in a cluster on the road. To account for a *doubly* stochastic property of the VANET, we first model vehicle's random locations as a stationary *Cox process* with *Fox's H-distributed* random intensity (vehicle concentration) and derive the distributional functions of the ℓth nearest client's distance from the beacon in such a Fox Cox field of vehicles. We then consolidate this spatial randomness of receiving vehicles into a path loss model and develop a *triply-composite* Fox channel model that combines key wireless propagation effects such as the distance-dependent path loss, large-scale fading (shadowing), and small-scale fading (multipath fading). In Fox channel modeling, each constituent propagation effect is described as Fox's H-variate, culminating again in Fox's H-variate for the received power or equivalently the instantaneous signal-to-noise ratio at the ℓth nearest client vehicle. Due to versatility of Fox's H-functions, this stochastic channel model can encompass a variety of well-established or generalized statistical propagation models used in wireless communication; be well-fitted to measurement data in diverse propagation environments by varying parameters; and facilitate a unifying analysis for fundamental physical-layer performances, such as error probability and channel capacity, using again the language of Fox's H-functions. This work serves to develop a unifying framework to characterize V2V communication in a doubly stochastic VANET by averaging both the small- and large-scale fading effects as well as the (random) distance-dependent path losses.**

***Index Terms*—Channel capacity, Cox process, Fox's H-variate, multipath fading, path loss, shadowing, symbol error probability (SEP), traffic flow theory, vehicle-to-vehicle (V2V) communication, vehicular ad-hoc network (VANET).**

Manuscript received March 1, 2012; revised July 23, 2012.

Y. Jeong and H. Shin (corresponding author) are with the Department of Electronics and Radio Engineering, Kyung Hee University, 1732 Deogyeong-daero, Giheung-gu, Yongin-si, Gyeonggi-do, 446-701 Korea (e-mail: yjeong@khu.ac.kr; hshin@khu.ac.kr). H. Shin is the corresponding author.

J. W. Chong and M. Z. Win are with the Laboratory for Information and Decision Systems (LIDS), Massachusetts Institute of Technology, 77 Massachusetts Avenue, Cambridge, MA 02139 USA (e-mail: jwchong@mit.edu; moewin@mit.edu).

This research was supported, in part, by the Basic Science Research Program through the National Research Foundation of Korea (NRF) funded by the Ministry of Science, ICT and Future Planning (2009-0083495), and NRF-2011-220-D00076 by the Ministry of Education.

Digital Object Identifier 10.1109/JSAC.2013.SUP.0513038

I. Introduction

As the demands for vehicle safety increase, a vehicular ad-hoc network (VANET) technology has been highlighted as a promising solution for preventing vehicle accidents. Car manufacturers, mobile network operators, and engineering communities are engrossed in developing and implementing such VANET technologies. For example, the U.S. Federal Communication Commission has allocated the 5.9-GHz dedicated short range communication (DSRC) spectrum for the exclusive use of vehicle-to-vehicle (V2V) and vehicle-to-infrastructure communications. To specify physical layer and medium access control technologies for DSRC, the IEEE 802.11p was organized and adjusted the IEEE 802.11a technology with low overhead operation [1], [2]. The higher layers, e.g., resource management, based on the IEEE 802.11p, are standardized by the IEEE 1609 working group [3]. In particular, safety message dissemination in the VANET requires V2V communication with—*low latency* and *high reliability*. However, the dynamics of vehicle passing and queueing as well as high mobility create distinctive propagation characteristics of wireless medium and rapid changes of network topology leading to inevitable uncertainty in space-time patterns of the vehicle density (concentration) on a road. Therefore, it is crucial to account for accurate wireless propagation characteristics as well as random vehicle locations in characterizing V2V communication.

Propagation model refinements for the V2V channel have been recently discussed by the measurement campaigns of the path loss, large-scale fading (shadowing), and small-scale fading (multipath fading) in highway, rural, urban, and/or suburban environments [4]–[12]. The measurement data have unveiled that the large-scale characteristics such as the path loss exponent (i.e., the slope of distance-dependent power loss in decibels (dB) for the standard power-law model) and shadowing parameter (i.e., the standard deviation of power loss in dB) are less severe than typical mobile communication cases [4]–[8]. Since vehicles act as reflectors and/or scatterers in intervehicle communication and transitions between line-of-sight (LOS) and non-LOS conditions occur often due to high mobility, the LOS is frequently lost and small-scale fading becomes more severe [9], [10]. A large amount of measurement data for small-scale fading in the 5-GHz-band V2V channel has been fitted to Weibull fading for 1, 5, 10, 20, 33.33, and 50 MHz channel bandwidth, evidencing that multipath fading is not always well described by typical models (e.g., Rayleigh or Nakagami-m) used for mobile communications and often worse than Rayleigh fading [11], [12]. However, these Weibull fits still exhibit a skew in agreement with the measurement data, which motivates a new class of statistical models for

V2V multipath fading.

The random space-time pattern of vehicle density (concentration) on a road is one of inevitable uncertainty in design and analysis of a vehicular network. This spatial and temporal (or doubly) stochastic characteristics are largely involved in traffic dynamics that has long been of interest due to its self-evident motivation since the 1930s. The seminal work of [13], [14] laid the early foundations on traffic flow theory, which states the relationship between the traffic flow, speed, and density as well as the capacity and delay of road systems.[1] In addition to this fundamental relationship between the traffic flow and density, the stochastic point process is an essential mathematical machinery to describe random locations of vehicles in the VANET [18]. The random-location modeling of vehicles in terms of the point processes enables to characterize spatial average of networking in a probabilistic framework and treats the VANET as a snapshot of a stationary random field of communicating vehicles, where the vehicle locations are viewed as the realizations of a point process. In particular, a *Cox process* (also known as a doubly stochastic Poisson process) can capture an unobserved *random heterogeneity* of vehicle spatial concentration on the road [19], [20]—which is a generalization of a Poisson point process (PPP) extensively used to describe spatial node distributions in a variety of wireless networks (see, e.g., [21]–[26] and reference therein).

In this paper, we consider a *doubly* stochastic VANET, where a beacon (or head) vehicle broadcasts safety application messages to neighboring client vehicles in a cluster $\mathcal{V}$ on the road. Specifically, we embody spatial randomness of client vehicles according to a stationary Cox process with Fox's H-distributed random intensity (vehicle density) to model a random distance of the ℓth nearest client from the beacon. We then consolidate this spatial randomness of receiving vehicles into a path loss model with accounting for the uncertainty in a transmission distance and develop a *composite Fox* channel model that integrates key wireless propagation effects such as the path loss, shadowing, and multipath fading. In Fox channel modeling, each ingredient propagation effect is described as Fox's H-variate, culminating again in Fox's H-variate for the received power or instantaneous signal-to-noise ratio (SNR) at the ℓth nearest client vehicle. The Fox's H-distribution is a general form spanning a large number of well-established nonnegative distributions, e.g., exponential, gamma, beta, Rayleigh, Nakagami-m, Weibull, and chi-square distributions (see also Table II) as special cases, and easily evolved under the Mellin transform leading to a tractable treatment of products, powers, and quotients of independent Fox's H-variates—referred to as the *H-preserving property* [27].[2] These properties serve to motivate using Fox H-distributions for statistical models for the vehicle spatial density as well as small- and large-scale wireless propagation characteristics. Due to the multifaceted nature of Fox's H-functions, the benefits of this stochastic channel model are three-fold: it can i) encompass a large variety of well-established or generalized statistical propagation models used in wireless communication; ii) be well-fitted to measurement data in diverse propagation environments by varying parameters; and iii) facilitate a unifying analysis for fundamental physical layer performances, such as error probability and channel capacity, using again the language of Fox's H-functions. The main contributions of this paper can be summarized as follows.

- *Cox spatial modeling:* Using stationary Cox processes, we first model random locations of client vehicles in the cluster $\mathcal{V}$, where a versatile family of statistical distributions (see Definition 1) is chosen for general statistical modeling (Fox's H-variate) of vehicle concentration. We then derive the distributional function of the ℓth nearest client's distance from the beacon vehicle in such a Fox Cox field of vehicles in terms of again Fox's H-distribution (see Theorem 1). This spatial model is well-diversified including as special cases: i) *negative binomial* vehicles for the gamma-distributed vehicle concentration (see Corollary 1) and ii) *Poisson* vehicles for the deterministic vehicle concentration (see Remark 2).
- *Fox channel modeling:* Using Fox's H-distributions, we put forth a stochastic V2V propagation model for intervehicle communication with accounting for the path loss, shadowing, and multipath fading as well as a random distance of communication links. We begin by modeling individual propagation effects in terms of Fox's H-variates (see Examples 2 and 3). We then develop a *triply-composite* Fox channel model for the instantaneous SNR at the ℓth nearest client vehicle by integrating them into a single compound H-variate using the H-preserving property under products, powers, quotients, and their combinations (see Theorem 2). As special cases, we particularize the orders and parameters of Fox's H-SNR for negative binomial and Poisson vehicles (see Corollary 2 and Remark 4).
- *Error probability and channel capacity:* Using the language of Fox's H-functions, we establish a unifying framework to analyze the error probability and channel capacity for intervehicle communication in a Cox field of vehicles. Specifically, the average symbol error probability (SEP), ergodic capacity, and outage capacity at the ℓth nearest client vehicle are derived in terms of Fox's H-functions (see Theorems 3–5). We further show that the high-SNR slope of the SEP is a function of only (a subset of) Fox's H-parameters of the instantaneous SNR (see Corollary 3).

The rest of the paper is organized as follows. In Sections II and III, we present the Cox spatial model and Fox channel model, respectively. Using the Cox-Fox model, the error probability and channel capacity are analyzed in Section IV for V2V communication in the doubly stochastic VANET and conclusions are finally given in Section V. The notation and symbols used in the paper are tabulated in Table I. We also adopt the convention of using letters without serifs for random variables.

[1]Subsequent to these early work, more than 100 traffic models have been suggested [15]–[17]: fluid-dynamic and car-following models [15], and cellular automata and nonlinear dynamics models [16], for example.

[2]Fox's H-distribution is based on the transcendental H-function first introduced by Fox [28]. Fox's H-function has recently found its vast potential of applications in a variety of science and engineering fields, e.g., reaction-diffusion, communication, fractional calculus, and statistical distribution theory [29]–[31].

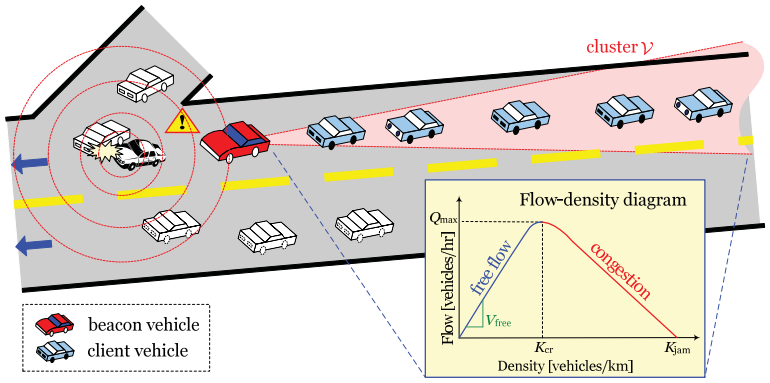

Fig. 1. Safety message dissemination in a vehicular network: a beacon vehicle broadcasts safety messages to neighboring client vehicles randomly located in a local cluster $\mathcal{V}$ on a road, where the traffic state is determined by the fundamental diagram of traffic flow.

II. Cox Spatial Modeling

We consider safety message dissemination in a VANET, as illustrated in Fig. 1, where a *beacon* (or head) vehicle operating in a sectorized transmission mode broadcasts safety or warning messages to neighboring *client* (or slave) vehicles randomly located in a local cluster $\mathcal{V}$ on a road.

A. Cox Field of Vehicles

Since the geometry of vehicle locations determines the signal strength (power) at each client vehicles, it plays a key role in characterizing intervehicle communication, especially for rapidly changing network topology due to high mobility. A complete solution to spatial modeling of vehicle locations in the VANET will involve a large number of statistical modeling issues concerned with both spatial and temporal aspects of this problem. The main factors that determine vehicle concentration (density), i.e., the number of vehicles per unit roadway length (e.g., km) are: i) the vehicle speed and traffic flow which depend on a traffic signal system regulating the passing and queueing of vehicles under speed limit constraints; and ii) a human factor called driver's response to stimuli [17]. The random variations of these factors cause uncertainty in the vehicle concentration.

Since the road traffic is *doubly* random—in space and in time—and vehicle moving is largely constrained to be one-dimensional due to static roadway geometry, the vehicles in the cluster $\mathcal{V}$ are assumed to be scattered according to a one-dimensional doubly stochastic point process Ψ with the intensity process $\Lambda(x)$, $x \in \mathbb{R}$. Conditioned on the random function $\Lambda(x)$, the vehicle positions in the VANET can be modeled as random points using a PPP, which has been used to describe spatial node distributions in wireless networks [21]–[26]. This highly motivates to use a Cox process for the vehicle spatial process Ψ. The Cox process Ψ is a generalization of PPPs, where the intensity $\Lambda(x)$ is itself a nonnegative stochastic process that models an unobserved random heterogeneity and the process Ψ conditional on $\Lambda(x)$ is a PPP with intensity function $\Lambda(x)$ [19], [20]. The beacon vehicle (transmitter) is deterministically located at the origin of the coordinate system, while the client vehicles (receivers) in the cluster $\mathcal{V}$ are on the road according to a one-dimensional stationary Cox process Ψ with the random vehicle density $\Lambda(x)$. Specifically, we consider a simple Cox process where $\Lambda(x)$ is equal to the same nonnegative random variable Λ for all locations $x \in \mathbb{R}_+$.[3] If Λ is deterministic, then the process Ψ boils down to simply a homogeneous Poisson process.

B. Vehicle Concentration Distributions

The traffic dynamics has long been of interest due to its self-evident motivation as the volume of vehicle traffic is ever-increasing under limitations of the roadway capacity. Subsequent to early foundations on traffic flow theory [13], [14], a number of attempts to solving the macroscopic traffic dynamics have been reported in the areas of engineering and statistical physics (see, e.g., [15]–[17] and references therein). In traffic flow theory, the relationship among speed, flow, and density is fitted to the fluid-dynamic equation for a traffic stream model and forms the so-called fundamental diagram of traffic flow [15], [16]. In particular, the flow-density diagram serves to determine the traffic state of the roadway (see Fig. 1). We can make the following remarks on the relationship between traffic flow [vehicles/hr] and density [vehicles/km].

- *Free flow region:* At low density, the flow almost linearly increases with a slope of free velocity V_{free} [km/hr] and reaches its maximum value $Q_{\max}$ [vehicles/hr] at the critical density K_{cr} [vehicles/km], which is the maximum density under the free-flow condition.
- *Congestion region:* At high density ($> K_{\text{cr}}$), the flow monotonically decreases (the higher the density, the lower the flow) and vanishes at the jam density K_{jam}, which is the minimum density under the congestion condition. The negative slope reflects the fact that the number of vehicles passing a point reduces due to limitation of the roadway capacity ($Q_{\max}$) even though there are more vehicles on the road.

This triangular shape of the flow-density diagram suggests to model the number of vehicles passing in a certain time interval and the number of vehicles being on a certain road length as the same class of distributions. For example, since

[3]This simplest case is often called a *mixed* Poisson process. The most prevalent and important example due to [34] is a gamma-distributed intensity $\Lambda \sim \text{Gamma}(\alpha, \beta)$ leading the mixed Poisson distribution to the negative binomial $\mathcal{NB}(\alpha, \frac{\beta}{\beta+1})$.

TABLE I
NOTATION AND SYMBOLS

$\mathbb{R}$	Real numbers
$\mathbb{R}_+$	Nonnegative real numbers
$\mathbb{Z}_+$	Nonnegative integers
$\mathbb{E}\{\cdot\}$	Expectation operator
$\mathbb{P}\{\cdot\}$	Probability measure
$p_X(x)$	Probability density function of X
$F_X(x)$	Cumulative distribution function of X
$\phi_X(s)$	Moment generating function of X: $\phi_X(s) = \mathbb{E}\{\exp(-sX)\}$
$\mathcal{N}(\mu, \sigma^2)$	Real Gaussian distribution with mean μ and variance σ^2
$\mathsf{Gamma}(\alpha, \beta)$	Gamma distribution with shape parameter $\alpha > 0$ and scale parameter $\beta > 0$: if $X \sim \mathsf{Gamma}(\alpha, \beta)$, then $p_X(x) = \frac{x^{\alpha-1}}{\Gamma(\alpha)\beta^\alpha} e^{-x/\beta}, \quad x \geq 0$
$\mathsf{Erl}(n, \lambda)$	nth-order Erlang distribution with hazard rate λ: if $X \sim \mathsf{Erl}(n, \lambda)$, then $p_X(x) = \frac{\lambda^n}{(n-1)!} x^{n-1} e^{-\lambda x}, \quad x \geq 0$
$\mathsf{Poisson}(\lambda)$	Poisson distribution with mean λ: if $X \sim \mathsf{Poisson}(\lambda)$, then $\mathbb{P}\{X = x\} = \frac{\lambda^x}{x!} e^{-\lambda}, \quad x \in \mathbb{Z}_+$
$\mathcal{NB}(r, p)$	Negative binomial (or Pólya) distribution with mean $\frac{pr}{1-p}$ and variance $\frac{pr}{(1-p)^2}$: if $X \sim \mathcal{NB}(r, p)$, then $\mathbb{P}\{X = x\} = \frac{\Gamma(x+r)}{x!\Gamma(r)} (1-p)^r p^x, \; x \in \mathbb{Z}_+$
$X \dot{\sim}$	X is approximated distributed as
$X \overset{\|Y}{\sim}$	X conditioned on Y is distributed as
$\overset{\mathrm{d}}{=}$	Distributional equality
$\doteq$	Asymptotically exponential equality: $f(x) \doteq x^y \;\Leftrightarrow\; \lim_{x\to\infty} \frac{\log f(x)}{\log x} = y$
$\boldsymbol{x}^{(i:j)}$	(i,j)th subvector of $\boldsymbol{x} = (x_1, x_2, \ldots, x_n)$: $\boldsymbol{x}^{(i:j)} = (x_i, x_{i+1}, \ldots, x_j)$
$\mathbf{1}_N$	N-dimensional all-one vector
$\Gamma(\cdot)$	Euler's Gamma function: $\Gamma(z) = \int_0^\infty t^{z-1} e^{-t} dt$
$K_\nu(\cdot)$	Modified Bessel function of the second kind [32, eq. (8.407.1)]
$G^{m,n}_{p,q}(\cdot)$	Meijer's G-function [33, eq. (8.2.1.1)]
$H^{m,n}_{p,q}[\cdot]$	Fox's H-function [33, eq. (8.3.1.1)]
$H^{\mathcal{L},n_1,n_2,m_1,m_2}_{\mathcal{M},(p_1:p_2),\mathcal{N},(q_1:q_2)}[\cdot]$	Fox's H-function of two variables [29, eq. (2.2.1)]

the traffic flow is fitted more accurately to a negative binomial distribution for high-variant traffic over both peak and off-peak periods [17], the number of vehicles on the road can be also modeled as a negative binomial variable.[4] In this case, from the widely-known property of negative binomial processes [34], [35] (see also Corollary 1), we can consider gamma distributions for vehicle concentration Λ in the Cox spatial modeling.

We begin by introducing a versatile family of statistical distributions for general distributional modeling of vehicle concentration Λ.

Definition 1 (Fox's H-Variates [27]): A nonnegative random variable X is said to have the (m, n, p, q)-order H-distribution with a parameter sequence $\mathcal{P} = (\kappa, c, \boldsymbol{a}, \boldsymbol{b}, \boldsymbol{\mathcal{A}}, \boldsymbol{\mathcal{B}})$, denoted by $X \sim \mathcal{H}^{m,n}_{p,q}(\mathcal{P})$, if its probability density function (PDF) is given by

$$p_X(x) = \kappa H^{m,n}_{p,q}\left[cx \,\middle|\, \begin{matrix} (a_1, \mathcal{A}_1), (a_2, \mathcal{A}_2), \ldots, (a_p, \mathcal{A}_p) \\ (b_1, \mathcal{B}_1), (b_2, \mathcal{B}_2), \ldots, (b_q, \mathcal{B}_q) \end{matrix}\right] \tag{1}$$

for $x \geq 0$, where the parameters κ, c, $\boldsymbol{a} = (a_1, a_2, \ldots, a_p)$, $\boldsymbol{b} = (b_1, b_2, \ldots, b_q)$, $\boldsymbol{\mathcal{A}} = (\mathcal{A}_1, \mathcal{A}_2, \ldots, \mathcal{A}_p)$, and $\boldsymbol{\mathcal{B}} = (\mathcal{B}_1, \mathcal{B}_2, \ldots, \mathcal{B}_q)$ have the values satisfying a distributional structure such that $\int_0^\infty p_X(x)\, dx = 1$, i.e.,

$$\frac{\kappa}{c} \frac{\prod_{j=1}^m \Gamma(b_j + \mathcal{B}_j) \prod_{j=1}^n \Gamma(1 - a_j - \mathcal{A}_j)}{\prod_{j=m+1}^q \Gamma(1 - b_j - \mathcal{B}_j) \prod_{j=n+1}^p \Gamma(a_j + \mathcal{A}_j)} = 1. \tag{2}$$

Remark 1: Fox's H-distribution can span a wide range of well-established distributions, e.g., exponential, Rayleigh, Nakagami-m, gamma, beta, chi-square, Weibull, and half-normal distributions as special cases. Moreover, it has the tractable (H-preserving) property to treat various combinations of products, powers, and quotients of independent Fox's H-variates [27].

For notational simplicity, we denote the right-hand side of (1) by $H^{m,n}_{p,q}(x; \mathcal{P})$. We get the following statistical properties of the Fox's H-distribution from basic identities of Fox's H-functions [30], [31], which will be useful in the paper.

Property 1 (CDF): The cumulative distribution function (CDF) of $X \sim \mathcal{H}^{m,n}_{p,q}(\mathcal{P})$ is given by

$$F_X(x) = 1 - H^{m+1,n}_{p+1,q+1}(x; \mathcal{P}_{\mathsf{cdf}}), \quad x \geq 0 \tag{3}$$

with the parameter sequence

$$\mathcal{P}_{\mathsf{cdf}} = \left(\frac{\kappa}{c}, c, (\boldsymbol{a} + \boldsymbol{\mathcal{A}}, 1), (0, \boldsymbol{b} + \boldsymbol{\mathcal{B}}), (\boldsymbol{\mathcal{A}}, 1), (1, \boldsymbol{\mathcal{B}})\right). \tag{4}$$

Property 2 (MGF): The moment generating function (MGF) of $X \sim \mathcal{H}^{m,n}_{p,q}(\mathcal{P})$ is given by

$$\phi_X(s) = H^{n+1,m}_{q,p+1}(s; \mathcal{P}_{\mathsf{mgf}}) \tag{5}$$

with the parameter sequence

$$\mathcal{P}_{\mathsf{mgf}} = \left(\frac{\kappa}{c}, \frac{1}{c}, (\mathbf{1}_q - \boldsymbol{b} - \boldsymbol{\mathcal{B}}), (0, \mathbf{1}_p - \boldsymbol{a} - \boldsymbol{\mathcal{A}}), \boldsymbol{\mathcal{B}}, (1, \boldsymbol{\mathcal{A}})\right). \tag{6}$$

Property 3 (Moment): The ith moment of $X \sim \mathcal{H}^{m,n}_{p,q}(\mathcal{P})$ is given by

$$\mathbb{E}\{X^i\} = \frac{\kappa}{c^{i+1}} \frac{\prod_{j=1}^m \Gamma(b_j + (i+1)\mathcal{B}_j)}{\prod_{j=n+1}^p \Gamma(a_j + (i+1)\mathcal{A}_j)} \times \frac{\prod_{j=1}^n \Gamma(1 - a_j - (i+1)\mathcal{A}_j)}{\prod_{j=m+1}^q \Gamma(1 - b_j - (i+1)\mathcal{B}_j)}. \tag{7}$$

Property 4 (Scaling): Let $Y = gX$ where $X \sim \mathcal{H}^{m,n}_{p,q}(\mathcal{P})$ and $g > 0$ is a constant. Then,

$$Y \sim \mathcal{H}^{m,n}_{p,q}\left(\tilde{\mathcal{P}} = \left(\frac{\kappa}{g}, \frac{c}{g}, \boldsymbol{a}, \boldsymbol{b}, \boldsymbol{\mathcal{A}}, \boldsymbol{\mathcal{B}}\right)\right). \tag{8}$$

Theorem 1 (Fox's H Vehicle Concentration): Let $\mathcal{L}(r) \subset \mathbb{R}_+$ be a Borel set $[0, r]$ of $\mathbb{R}$ (r-length roadway) and let client vehicles in the cluster $\mathcal{V}$ belong to a Cox process Ψ with the

[4] A variety of disturbing factors (e.g., traffic signals) in the VANET can cause large variations of the vehicle concentration in space and time domains.

$$
\begin{aligned}
p_{R_\ell}(r) &= \frac{r^{\ell-1}}{(\ell-1)!}\int_0^\infty \lambda^\ell e^{-\lambda r} H_{p,q}^{m,n}(\lambda;\mathcal{P})\,d\lambda \\
&= \frac{\mathcal{K}}{r^2(\ell-1)!} H_{p+1,q}^{m,n+1}\left[\frac{c}{r}\,\middle|\,\begin{matrix}(-\ell,1),(a_1,\mathcal{A}_1),(a_2,\mathcal{A}_2),\ldots,(a_p,\mathcal{A}_p)\\ (b_1,\mathcal{B}_1),(b_2,\mathcal{B}_2),\ldots,(b_q,\mathcal{B}_q)\end{matrix}\right] \\
&= \frac{\mathcal{K}}{c^2(\ell-1)!} H_{q,p+1}^{n+1,m}\left[\frac{r}{c}\,\middle|\,\begin{matrix}(1-b_1-2\mathcal{B}_1,\mathcal{B}_1),\ldots,(1-b_q-2\mathcal{B}_q,\mathcal{B}_q)\\ (\ell-1,1),(1-a_1-2\mathcal{A}_1,\mathcal{A}_1),\ldots,(1-a_p-2\mathcal{A}_p,\mathcal{A}_p)\end{matrix}\right]
\end{aligned} \tag{13}
$$

vehicle density $\Lambda \sim \mathcal{H}_{p,q}^{m,n}(\mathcal{P})$. Then, the probability that ℓ client vehicles are on $\mathcal{L}(r)$, $\ell \in \mathbb{Z}_+$, is given by

$$
\begin{aligned}
&\mathbb{P}\{\ell \text{ vehicles on } \mathcal{L}(r)\} \\
&= \frac{\mathcal{K}}{r\ell!} H_{p+1,q}^{m,n+1}\left[\frac{c}{r}\,\middle|\,\begin{matrix}(-\ell,1),(a_1,\mathcal{A}_1),\ldots,(a_p,\mathcal{A}_p)\\ (b_1,\mathcal{B}_1),\ldots,(b_q,\mathcal{B}_q)\end{matrix}\right].
\end{aligned} \tag{9}
$$

The ℓth nearest client vehicle's distance R_ℓ from the beacon vehicle at the origin is Fox's H-variate $R_\ell \sim \mathcal{H}_{q,p+1}^{n+1,m}(\mathcal{P}_\ell)$ with the parameter sequence

$$
\begin{aligned}
\mathcal{P}_\ell = \Bigg(&\frac{\mathcal{K}}{c^2(\ell-1)!}, \frac{1}{c}, \mathbf{1}_q - \boldsymbol{b} - 2\boldsymbol{\mathcal{B}}, \\
&\left(\ell-1, \mathbf{1}_p - \boldsymbol{a} - 2\boldsymbol{\mathcal{A}}\right), \boldsymbol{\mathcal{B}}, (1,\boldsymbol{\mathcal{A}})\Bigg).
\end{aligned} \tag{10}
$$

Proof: Since $\mathbb{P}\{\ell \text{ vehicles on } \mathcal{L}(r)|\,\Lambda\} = \frac{(\Lambda r)^\ell}{\ell!}e^{-\Lambda r}$, it follows from the law of total probability that

$$
\begin{aligned}
\mathbb{P}\{\ell \text{ vehicles on } \mathcal{L}(r)\} &= \int_0^\infty \frac{(\lambda r)^\ell}{\ell!} e^{-\lambda r} dF_\Lambda(\lambda) \\
&= \frac{r^\ell}{\ell!}\int_0^\infty \lambda^\ell e^{-\lambda r} H_{p,q}^{m,n}(\lambda;\mathcal{P})\,d\lambda.
\end{aligned} \tag{11}
$$

With the help of the identity [33, eq. (2.25.1.1)], we arrive at the desired result (9).

Using (11), the CDF of R_ℓ can be written as

$$
\begin{aligned}
F_{R_\ell}(r) &= 1 - \mathbb{P}\{0,1,\ldots,\ell-1 \text{ vehicles on } \mathcal{L}(r)\} \\
&= 1 - \int_0^\infty \left(\sum_{i=0}^{\ell-1}\frac{(\lambda r)^i}{i!}\right) e^{-\lambda r} H_{p,q}^{m,n}(\lambda;\mathcal{P})\,d\lambda.
\end{aligned} \tag{12}
$$

By differentiating (12) with respect to r, after some manipulations, we obtain (13), where the last equality follows from the identities [31, eqs. (1.58) and (1.60)]. □

Corollary 1 (Gamma Vehicle Concentration): Let $\Lambda \sim \mathrm{Gamma}(\alpha_\mathrm{v}, \beta_\mathrm{v})$. Then, the number of client vehicles being on the Borel set $\mathcal{L}(r)$, denoted by $V(r)$, is the negative binomial variable

$$
V(r) \sim \mathcal{NB}\left(\alpha_\mathrm{v}, \frac{\beta_\mathrm{v} r}{\beta_\mathrm{v} r + 1}\right) \tag{14}
$$

and the PDF of the ℓth nearest distance R_ℓ in a gamma Cox field of vehicles is given by

$$
p_{R_\ell}(r) = \frac{\beta_\mathrm{v}}{(\ell-1)!\Gamma(\alpha_\mathrm{v})} H_{1,1}^{1,1}\left[\beta_\mathrm{v} r\,\middle|\,\begin{matrix}(-\alpha_\mathrm{v},1)\\ (\ell-1,1)\end{matrix}\right], \quad r \geq 0 \tag{15}
$$

that is, $R_\ell \sim \mathcal{H}_{1,1}^{1,1}(\mathcal{P})$ with the parameter sequence

$$
\mathcal{P} = \left(\frac{\beta_\mathrm{v}}{(\ell-1)!\Gamma(\alpha_\mathrm{v})}, \beta_\mathrm{v}, -\alpha_\mathrm{v}, \ell-1, 1, 1\right). \tag{16}
$$

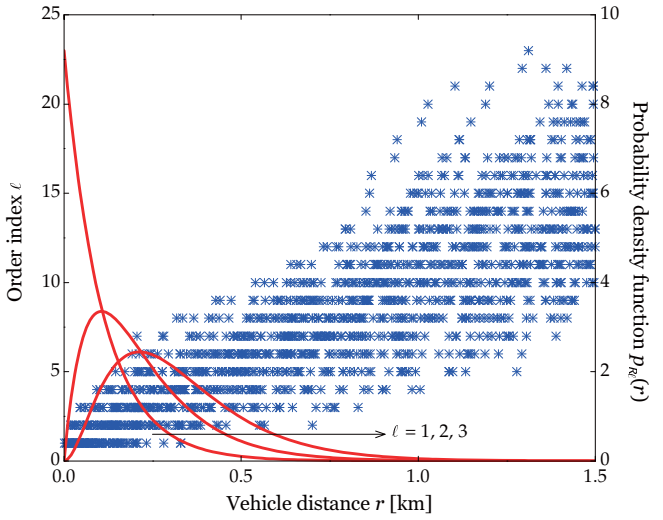

Fig. 2. (Snapshot) 100 realizations (blue marks) of the ℓth nearest vehicle positions R_ℓ in a Cox process Ψ with the gamma vehicle concentration $\Lambda \sim \mathrm{Gamma}(51.9354, 0.1770)$ vehicles/km. The PDF $p_{R_\ell}(r)$ of the ℓth nearest distance R_ℓ in this gamma Cox field of vehicles is also plotted for $\ell = 1$, 2, and 3 using Corollary 1 (red solid lines).

Proof: It follows readily from the fact that

$$
\begin{aligned}
&\Lambda \sim \mathrm{Gamma}(\alpha_\mathrm{v}, \beta_\mathrm{v}) \\
&\overset{\mathrm{d}}{=} \mathcal{H}_{0,1}^{1,0}\left(\mathcal{P}_\mathrm{g} = \left(\frac{1}{\beta_\mathrm{v}\Gamma(\alpha_\mathrm{v})}, \frac{1}{\beta_\mathrm{v}}, -, \alpha_\mathrm{v}-1, -, 1\right)\right)
\end{aligned} \tag{17}
$$

and Theorem 1. □

Remark 2 (Deterministic Vehicle Concentration): Let $\Lambda \sim \mathrm{Gamma}(\alpha_\mathrm{v}, \beta_\mathrm{v} = \lambda_0/\alpha_\mathrm{v})$. Then, as $\alpha_\mathrm{v} \to \infty$, we have $\Lambda = \lambda_0$ with probability one, leading to $V(r) \sim \mathrm{Poisson}(\lambda_0 r)$ and

$$
\begin{aligned}
&R_\ell \sim \mathrm{Erl}(\ell, \lambda_0) \\
&\overset{\mathrm{d}}{=} \mathcal{H}_{0,1}^{1,0}\left(\mathcal{P}_\mathrm{p} = \left(\frac{\lambda_0}{(\ell-1)!}, \lambda_0, -, \ell-1, -, 1\right)\right)
\end{aligned} \tag{18}
$$

as expected. In this case, the Cox process Ψ reduces to a homogeneous PPP with intensity λ_0.

Example 1 (Gamma Cox Field of Vehicles): Fig. 2 shows 100 snapshot realizations of the ℓth nearest vehicle positions in a Cox field Ψ with the gamma intensity $\Lambda \sim \mathrm{Gamma}(51.9354, 0.1770)$ vehicles/km for a cyclic-variant (or congested) traffic scenario. The PDF $p_{R_\ell}(r)$ of the ℓth nearest distance R_ℓ in this gamma Cox field of vehicles is also plotted for $\ell = 1$, 2, 3 using Corollary 1 (red solid lines). The traffic measurement data have justified that the negative binomial distribution is well-fitted to the flow for the cyclic-variant or congested traffic, whereas the Poisson fit is acceptable for the light traffic-only scenario [17]. For example, the

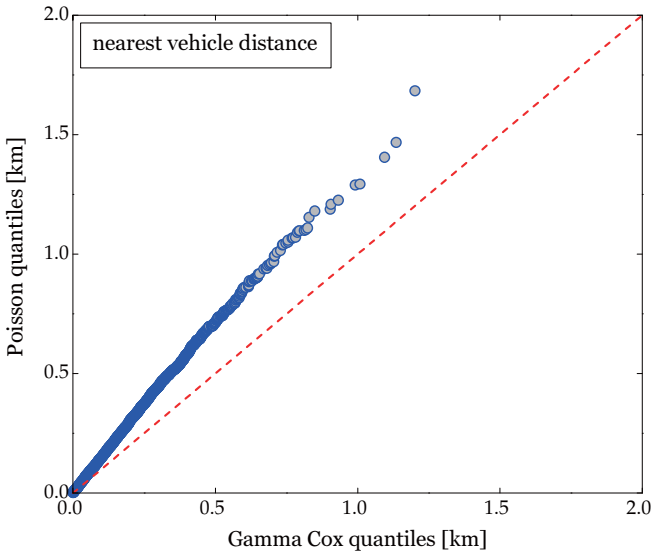

Fig. 3. Q-Q plot of the nearest vehicle distance R_1 [km] for the Cox process with the gamma vehicle concentration $\Lambda \sim \text{Gamma}\,(51.9354, 0.1770)$ vehicles/km (cyclic-variant traffic) and the Poisson process with $\lambda_0 = 6$ vehicles/km (light traffic).

traffic flow can be fitted to $\mathcal{NB}\,(5.7706, 0.1504)$ vehicles/10-sec from the measurement data in [17, Table 3.4], where it was remarked that this negative binomial fit is acceptable by a χ^2 test at 5 % significant level while the Poisson fit is not. Letting $V_{\text{free}} = 40$ km/hr in the flow-density diagram (Fig. 1), this negative binomial traffic flow is projected at the number of vehicles on the r-km road as $V\,(r\,\text{km}) \sim \mathcal{NB}\left(51.9354, \frac{0.1770r}{0.1770r+1}\right)$ vehicles in the free flow region. This corresponds in turn to the Cox process Ψ with the vehicle concentration $\Lambda \sim \text{Gamma}\,(51.9354, 0.1770)$ vehicles/km from Corollary 1. Fig. 3 shows the quantile-quantile (Q-Q) plot of the nearest vehicle distance R_1 for the gamma Cox process (cyclic-variant traffic) and the Poisson process with $\lambda_0 = 6$ vehicles/km (light traffic).[5] In this figure, the gamma Cox process produces $V\,(2\,\text{km}) \sim \mathcal{NB}\,(51.9354, 0.2614)$ vehicles for $r = 2$ km, while $V\,(2\,\text{km}) \sim \text{Poisson}\,(12)$ vehicles for the Poisson process. Since the Q-Q plot is steeper than the reference line (red dashed line), the Poisson vehicles are more dispersed than the negative binomial vehicles. Moreover, the Q-Q plot lies above the reference, meaning that the average nearest distance (166.7 m) for the Poisson vehicles is larger than 110.8 m for the negative binomial vehicles (gamma Cox).

III. Fox Channel Modeling

In this section, we describe a V2V propagation model for intervehicle communication in a random field of vehicles. The channel modeling for wireless communication is important for physical layer design to tailor fading countermeasures such as forward error correction, diversity transmission/reception, and equalization.

[5]The Q-Q plot is a probability plot to graphically compare two distributions by scattering their quantiles on the plot.

A. Wireless Propagation Characteristics

In design and analysis of a wireless network, the power relationship between the transmitter and receiver is necessary and sufficient to account for the propagation characteristics of wireless medium, such as path loss, shadowing, and multipath fading. Specifically, we consider that the received power P_{rx} at a client vehicle in $\mathcal{V}$ located at a distance R from the beacon vehicle is given by

$$P_{\text{rx}} = \frac{P_{\text{tx}}}{\eta} \cdot \frac{Z^2 X_\sigma}{R^\nu} \tag{19}$$

leading to the instantaneous symbol signal-to-noise ratio (SNR):[6]

$$\gamma = \frac{E_{\text{s}}}{\eta N_0} \cdot \frac{Z^2 X_\sigma}{R^\nu} \tag{20}$$

where P_{tx} is the transmit power at the beacon vehicle; η is the path loss measured at a reference distance of 1 meter away from the transmitter; E_{s} denotes the energy per symbol; N_0 is the power spectral density (PSD) of the additive white Gaussian noise; ν is the power loss exponent; X_σ is the (large-scale) shadowing with the standard deviation (shadowing parameter) σ of the instantaneous power; and Z is the envelope of multipath (small-scale) fading with $\mathbb{E}\left\{Z^2\right\} = 1$. The shadowing X_σ captures random fluctuations in the average signal power around the path loss $1/\left(\eta r^\nu\right)$ given that $R = r$ (client vehicle's distance), while the multipath effect Z is superimposed on the path loss and shadowing. This propagation model is well-diversified to account for key composite effects of small- and large-scale fading as well as the random communication distance due to spatial (location) randomness of the receiver.

1) Path Loss and Shadowing: The extensive measurement campaigns have been recently carried out to model the path loss and shadowing of the V2V channel in a variety of propagation environments such as highway, rural, urban, and/or suburban scenarios [4]–[7]. Since the V2V communication is highly ad-hoc and dynamic as well as straight ahead vehicles, buildings, vegetation and/or other roadside objects act as obstacles on signal propagation, the distance-dependent path loss and shadowing is important propagation effects in the V2V channel [7], [8]. These effects are typically modeled by a standard power decay law and a lognormal variable, leading to the power loss in decibels (dB) at a distance R from the transmitter as follows:

$$P_{\text{loss}}\,(R) = \eta\,[\text{dB}] + \nu \cdot 10\log_{10}(R) + \sigma_{\text{dB}} G \tag{21}$$

where $G \sim \mathcal{N}\,(0, 1)$ and $\sigma_{\text{dB}} = \sigma 10/\ln 10$ is the standard deviation of the received power in dB. The ranges of the power loss exponent ν for V2V channels can be: 1.8–1.9 in the highway and rural environments; and 1.6–1.7 in the urban environment [7]. The experimentally extracted values of $\eta\,[\text{dB}]$, ν, and σ_{dB} for urban and suburban environments in [6] are tabulated in Table II, which will be used for our numerical examples.[7]

[6]The average symbol energy E_{s} is equal to $E_{\text{s}} = P_{\text{av}}/R_{\text{s}}$, where P_{av} and R_{s} denote the average transmit power and symbol rate, respectively.

[7]Note that the reference distance was chosen to 10 meters in [6].

TABLE II
PATH LOSS AND SHADOWING PARAMETERS FOR V2V CHANNELS: EXPERIMENTAL MODELING AT 5.2 GHZ IN [6] AND FOX'S H-FITS TO LOGNORMAL SHADOWING X_σ.

Scenario	Path loss		Shadowing							
	Experimental modeling [6]			Fox's H-fit						
	η [dB]	ν	$\sigma_{\rm dB}$	$m\ n\ p\ q$	$\mathcal{k}$	c	$\boldsymbol{a}$	$\boldsymbol{b}$	$\mathcal{A}$	$\mathcal{B}$
Urban	45.2	1.68	1.7	1 0 0 1	4.79067×10^{-69}	173852	–	53.26	–	3
Suburban	48.7	1.59	2.1	1 0 0 1	3.93862×10^{-36}	45137.5	–	33.03	–	3

TABLE III
FOX'S H-EQUIVALENTS OF TYPICAL AND GENERALIZED STATISTICAL MODELS FOR SCALED MULTIPATH FADING Y.

Fading model	$m\ n\ p\ q$	$\mathcal{k}$	c	$\boldsymbol{a}$	$\boldsymbol{b}$	$\mathcal{A}$	$\mathcal{B}$
Rayleigh	1 0 0 1	$\sqrt{\frac{1}{\Omega}}$	$\sqrt{\frac{1}{\Omega}}$	–	$\frac{1}{2}$	–	$\frac{1}{2}$
Nakagami-m	1 0 0 1	$\frac{\sqrt{m/\Omega}}{\Gamma(m)}$	$\sqrt{\frac{m}{\Omega}}$	–	$m-\frac{1}{2}$	–	$\frac{1}{2}$
Weibull	1 0 0 1	$\sqrt{\frac{\Gamma(1+2/\beta)}{\Omega}}$	$\sqrt{\frac{\Gamma(1+2/\beta)}{\Omega}}$	–	$1-\frac{1}{\beta}$	–	$\frac{1}{\beta}$
α-μ (Stacy)	1 0 0 1	$\frac{1}{\Gamma(\mu)}\sqrt{\frac{\Gamma(\mu+2/\alpha)}{\Gamma(\mu)\Omega}}$	$\sqrt{\frac{\Gamma(\mu+2/\alpha)}{\Gamma(\mu)\Omega}}$	–	$\mu-\frac{1}{\alpha}$	–	$\frac{1}{\alpha}$
Generalized-K	2 0 0 2	$\frac{\sqrt{m_1 m_2/\Omega}}{\Gamma(m_1)\Gamma(m_2)}$	$\sqrt{\frac{m_1 m_2}{\Omega}}$	–	$(m_2-\frac{1}{2}, m_1-\frac{1}{2})$	–	$\frac{1}{2}\mathbf{1}_2$
$N*$Nakagami-m	N 0 0 N	$\prod_{i=1}^{N}\frac{\sqrt{m_i/\Omega_i}}{\Gamma(m_i)}$	$\prod_{i=1}^{N}\sqrt{\frac{m_i}{\Omega_i}}$	–	$(m_1-\frac{1}{2},\ldots,m_N-\frac{1}{2})$	–	$\frac{1}{2}\mathbf{1}_N$

The lognormal shadowing $X_\sigma = \exp(\sigma G)$ is often approximated to a gamma variate due to its analytic tractability as follows: [36], [37]

$$X_\sigma \dot{\sim} \text{Gamma}\left(\frac{1}{e^{\sigma^2}-1}, e^{\sigma^2/2}\left(e^{\sigma^2}-1\right)\right). \quad (22)$$

We use a family of the $(1,0,0,1)$-order H-variates with a parameter sequence

$$\hat{\mathcal{P}} = \left(\hat{\mathcal{k}}, \hat{c}, -, \hat{\boldsymbol{b}}, -, \hat{\mathcal{B}}\right) \quad (23)$$

to refine the approximation as

$$X_\sigma \dot{\sim} \mathcal{H}_{0,1}^{1,0}\left(\hat{\mathcal{P}}\right). \quad (24)$$

Using Property 3, we can determine the Fox's H-fit parameters by matching the first two moments exactly and the third moment as close as possible between the lognormal and Fox's H variables as follows:

$$\exp\left(\frac{i^2\sigma^2}{2}\right) = \frac{\hat{\mathcal{k}}}{\hat{c}^{i+1}}\Gamma\left(\hat{\boldsymbol{b}} + (i+1)\,\hat{\mathcal{B}}\right), \quad i = 0,1,2 \quad (25)$$

for given $\hat{\mathcal{B}}$ which is chosen to control the third moment.

Example 2 (Shadowing): Figs. 4 and 5 show the $(1,0,0,1)$-order H-fits to the lognormal shadowing experimentally parameterized for the urban ($\sigma_{\rm dB} = 1.7$) and suburban ($\sigma_{\rm dB} = 2.1$) modeling of the V2V channel at 5.2 GHz in Table II. For comparison, we also plot the gamma fits in the figures. Since these Fox's H-fits try to match up to the first three moments (i.e., mean, variance, and skewness) with the lognormal shadowing, the Fox's H-PDF gives a remarkably accurate approximation to the lognormal. Note that as $\hat{\mathcal{B}}$ increases, the Fox's H-fit becomes more accurate without any notable discrepancy.

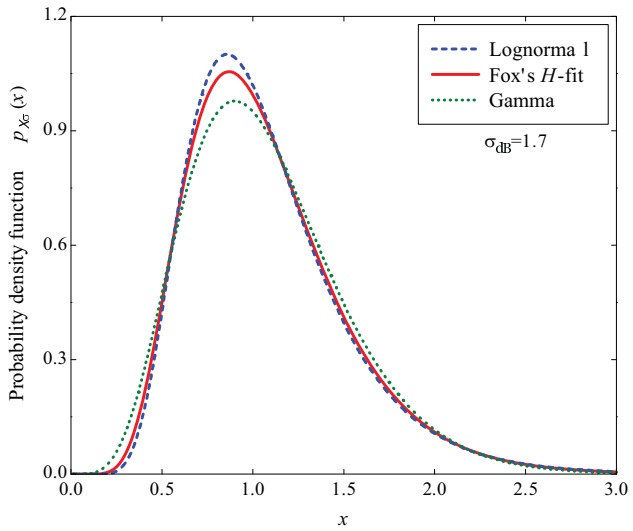

Fig. 4. $(1,0,0,1)$-order H-fit to lognormal shadowing X_σ with $\sigma_{\rm dB} = 1.7$ for urban modeling of the V2V channel at 5.2 GHz in Table II. For comparison, the gamma fit is also plotted.

2) Multipath Fading: Measurement and modeling campaigns have evidenced that the multipath fading of the V2V channel is not always well described by typical models (such as Rayleigh or Nakagami-m) and motivated a general stochastic fading model [10]–[12]. We first underline a class of general stochastic fading models well-suited for the V2V

channel and then put forward to use again Fox's H-distribution that can encompass all these generalized fading as special cases (see, e.g., Table III). Let $Y = \sqrt{\Omega}Z$ be a scaled fading envelop with $\mathbb{E}\{Y^2\} = \Omega$. We make the following reviews of the generalized fading for the V2V communication.

- α-μ *(Stacy) Fading:* In this fading model, the PDF of the scaled fading envelope Y is given by (26) [38], where $\hat{y} \triangleq \sqrt[\alpha]{\mathbb{E}\{Y^\alpha\}}$ is the α-root mean value; $\alpha > 0$ is the power parameter; $\mu > 0$ is the inverse of the normalized variance of Y^α; and $\Omega = \hat{y}^2 \mu^{-\frac{2}{\alpha}} \frac{\Gamma(\mu+2/\alpha)}{\Gamma(\mu)}$. This fading model accounts for the nonlinearity of propagation medium as well as the multipath wave clustering by rewriting the Stacy distribution in terms of two physical fading parameters α and μ reflecting the nonlinearity and clustering, respectively [38]–[41]. This model can span a wide range of small-scale fading such as Rayleigh ($\alpha = 2$, $\mu = 1$), Nakagami-m ($\alpha = 2$, $\mu = m$), and Weibull ($\mu = 1$) fading. In particular, a large amount of measurement data for small-scale fading in the 5-GHz-band V2V channel has been fitted to Weibull fading for 1, 5, 10, 20, 33.33, and 50 MHz channel bandwidth [11], [12]. A subset of Weibull fits is tabulated in Table IV.
- $N*$*Nakagami-*m *Fading:* This fading is constructed by the product of N statistically independent but not necessarily identically distributed Nakagami-m variables, yielding the PDF of the scaled fading envelope Y as (27) [42], where $m_i \geq 0.5$ and $\Omega_i > 0$ are the fading severity parameter and the mean power of the ith Nakagami-m fading component, respectively; and $\Omega = \prod_{i=1}^{N} \Omega_i$. For $N = 2$, this model well describes the V2V channel where two Nakagami-m fading processes are generated by independent clusters of scatterers around two vehicles [43]. In fact, this case is identical to the generalized-K fading which has been introduced to account for the composite effect of shadowing and small-scale random variations, giving the PDF of the scaled fading envelope Y as (28), where m_1 and $m_2 = 1/\left(e^{\sigma^2} - 1\right)$ are Nakagami parameters for multipath fading and shadowing, respectively. The generalized-K fading reduces to the K-fading for $m_1 = 1$ [36] and further to Rayleigh for $m_2 \to \infty$.

The expressions (26)–(28) for the generalized fading in terms of Fox's H-functions stimulate again to model multipath fading Y (or equivalently Z) of the V2V channel as Fox's H-variate.[8]

Example 3 (Multipath Fading): Figs. 6 and 7 show the $(3, 0, 0, 3)$-order H-fits to the measurements reported in [11, Fig. 8] and [10, Fig. 2] for multipath fading of the 5-GH-band V2V channel in Table IV. For comparison, the Weibull fits ($\beta = 1.61$ and $\beta = 1.66$) in [11] and [10] are also plotted. We observe again that Fox's H-modeling enables a more accurate fit to the measurement.

B. Fox Modeling

For V2V communication in a Cox field of vehicles, we now elaborate a Fox channel model composed of the path loss, shadowing, and multipath fading components, each with Fox's H-distribution.

[8]Using Property 4, it is immediate to get Fox's parameters for Z from its scaled form Y.

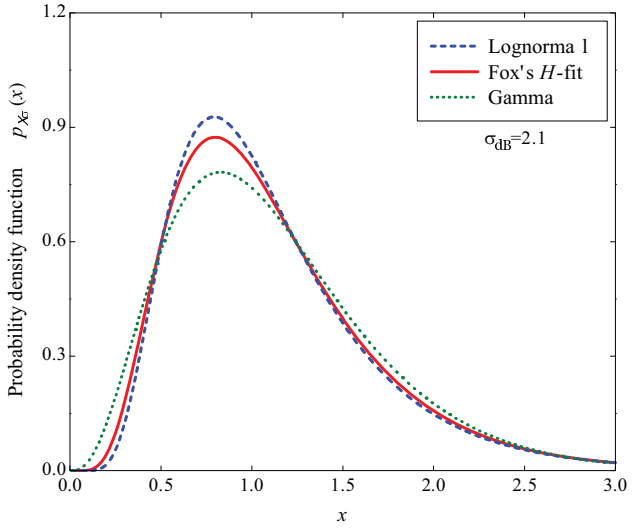

Fig. 5. $(1, 0, 0, 1)$-order H-fit to lognormal shadowing X_σ with $\sigma_{\mathrm{dB}} = 2.1$ for suburban modeling of the V2V channel at 5.2 GHz in Table II. For comparison, the gamma fit is also plotted.

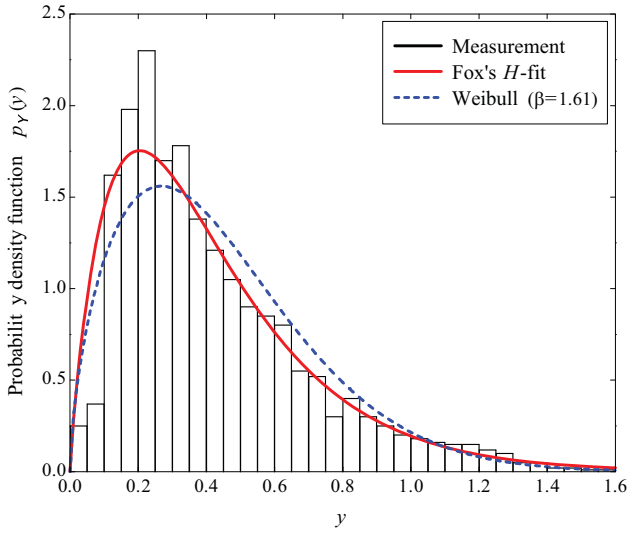

Fig. 6. $(3, 0, 0, 3)$-order H-fit to the measurement reported in [11, Fig. 8] for scaled multipath fading Y of the 5-GH-band V2V channel in Table IV (Data 1). For comparison, the Weibull fit ($\beta = 1.61$) in [11] is also plotted.

Theorem 2 (Cox–Fox V2V Channel): Let client vehicles in the cluster $\mathcal{V}$ belong to a Cox process Ψ with the vehicle density $\Lambda \sim \mathcal{H}^{m_{\mathrm{v}},n_{\mathrm{v}}}_{p_{\mathrm{v}},q_{\mathrm{v}}}(\mathcal{P}_{\mathrm{v}})$. Let $X_\sigma \sim \mathcal{H}^{m_{\mathrm{s}},n_{\mathrm{s}}}_{p_{\mathrm{s}},q_{\mathrm{s}}}(\mathcal{P}_{\mathrm{s}})$ and $Z \sim \mathcal{H}^{m_{\mathrm{m}},n_{\mathrm{m}}}_{p_{\mathrm{m}},q_{\mathrm{m}}}(\mathcal{P}_{\mathrm{m}})$ be the shadowing and multipath fading ingredients of the V2V channel, respectively. Then, the instantaneous SNR

$$\gamma_\ell = \frac{E_{\mathrm{s}}/N_0}{\eta} \cdot \frac{Z^2 X_\sigma}{R_\ell^\nu} \tag{29}$$

at the ℓth nearest client vehicle is Fox's H-variate $\gamma_\ell \sim \mathcal{H}^{m,n}_{p,q}(\mathcal{P})$ with the order

$$\begin{aligned}(m, n, p, q) = (&m_{\mathrm{v}} + m_{\mathrm{s}} + m_{\mathrm{m}}, n_{\mathrm{v}} + n_{\mathrm{s}} + n_{\mathrm{m}} + 1,\\ &p_{\mathrm{v}} + p_{\mathrm{s}} + p_{\mathrm{m}} + 1, q_{\mathrm{v}} + q_{\mathrm{s}} + q_{\mathrm{m}})\end{aligned} \tag{30}$$

$$p_Y(y) = \frac{\alpha\mu^{\mu} y^{\alpha\mu-1}}{\hat{y}^{\alpha\mu}\Gamma(\mu)} \exp\left(-\frac{\mu y^{\alpha}}{\hat{y}^{\alpha}}\right)$$
$$= \frac{\mu^{1/\alpha}}{\hat{y}\Gamma(\mu)} H_{0,1}^{1,0}\left[\frac{\mu^{1/\alpha} y}{\hat{y}} \,\middle|\, \begin{matrix} - \\ (\mu - 1/\alpha, 1/\alpha) \end{matrix}\right], \quad y \geq 0 \tag{26}$$

$$p_Y(y) = \frac{2}{y\prod_{i=1}^{N}\Gamma(m_i)} G_{0,N}^{N,0}\left(y^2 \prod_{i=1}^{N}\frac{m_i}{\Omega_i} \,\middle|\, \begin{matrix} - \\ m_1, m_2, \ldots, m_N \end{matrix}\right)$$
$$= \left(\prod_{i=1}^{N}\frac{\sqrt{m_i/\Omega_i}}{\Gamma(m_i)}\right) H_{0,N}^{N,0}\left[y\prod_{i=1}^{N}\sqrt{\frac{m_i}{\Omega_i}} \,\middle|\, \begin{matrix} - \\ (m_1 - \frac{1}{2}, \frac{1}{2}), \ldots, (m_N - \frac{1}{2}, \frac{1}{2}) \end{matrix}\right], \quad y \geq 0 \tag{27}$$

$$p_Y(y) = \frac{4(m_1 m_2/\Omega)^{(m_1+m_2)/2}}{\Gamma(m_1)\Gamma(m_2)} y^{m_1+m_2-1} K_{m_2-m_1}\left(2y\sqrt{\frac{m_1 m_2}{\Omega}}\right)$$
$$= \frac{\sqrt{m_1 m_2/\Omega}}{\Gamma(m_1)\Gamma(m_2)} H_{0,2}^{2,0}\left[y\sqrt{\frac{m_1 m_2}{\Omega}} \,\middle|\, \begin{matrix} - \\ (m_2 - \frac{1}{2}, \frac{1}{2}), (m_1 - \frac{1}{2}, \frac{1}{2}) \end{matrix}\right], \quad y \geq 0 \tag{28}$$

TABLE IV
FOX'S H-FITS TO MEASUREMENTS FOR SCALED MULTIPATH FADING Y OF THE 5-GHZ-BAND V2V CHANNEL.

Index	Weibull fit	Fox's H-fit						
	β	$m\ n\ p\ q$	k	c	$\boldsymbol{a}$	$\boldsymbol{b}$	$\boldsymbol{\mathcal{A}}$	$\boldsymbol{\mathcal{B}}$
Measurement 1	1.61 ($\Omega = 0.27$) [11, Fig. 8]	3 0 0 3	0.225	5.774	–	$(1.5, 0.4, 4.5)$	–	$\frac{1}{2}\mathbf{1}_3$
Measurement 2	1.66 ($\Omega = 0.19$) [10, Fig. 2]	3 0 0 3	2.874	3.940	–	$(0.45, 2, 1.8)$	–	$(\frac{1}{2}\mathbf{1}_2, 0.2)$

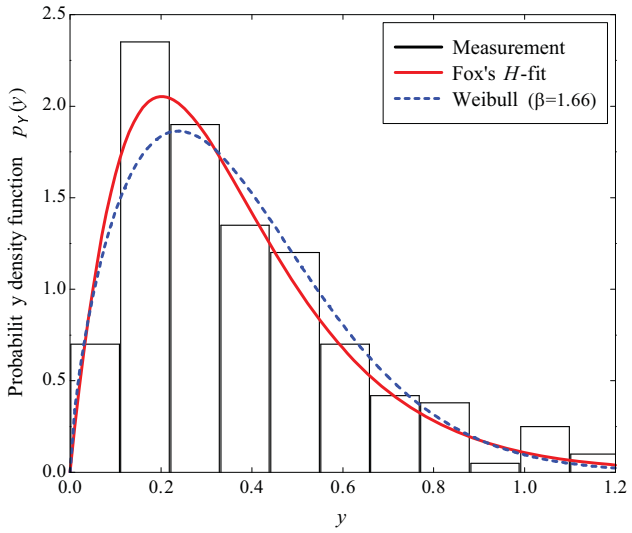

Fig. 7. $(3, 0, 0, 3)$-order H-fit to the measurement reported in [10, Fig. 2] for scaled multipath fading Y of the 5-GH-band V2V channel in Table IV (Data 2). For comparison, the Weibull fit ($\beta = 1.66$) in [10] is also plotted.

and the parameter sequence

$$\mathcal{P} = \left(\frac{\eta k_{\mathrm{v}} k_{\mathrm{s}} k_{\mathrm{m}} c_{\mathrm{v}}^{\nu-1} c_{\mathrm{m}}}{E_{\mathrm{s}}/N_0\,(\ell-1)!}, \frac{\eta c_{\mathrm{v}}^{\nu} c_{\mathrm{s}} c_{\mathrm{m}}^2}{E_{\mathrm{s}}/N_0}, \boldsymbol{a}, \boldsymbol{b}, \boldsymbol{\mathcal{A}}, \boldsymbol{\mathcal{B}}\right) \tag{31}$$

where the parameter sequences $\boldsymbol{a}, \boldsymbol{b}, \boldsymbol{\mathcal{A}}$, and $\boldsymbol{\mathcal{B}}$ are given by (32)–(35).

Proof: It follows readily from Property 4, Theorem 1, and [27, Theorems 4.1–4.3]. □

Remark 3 (Spatial Conditioning): Given $R_\ell = r$, the location-conditioned SNR at the client vehicle becomes $\gamma_\ell(r) \overset{|R}{\sim} \mathcal{H}_{p,q}^{m,n}(\mathcal{P}(r))$ with the order

$$(m, n, p, q) = (m_{\mathrm{s}} + m_{\mathrm{m}}, n_{\mathrm{s}} + n_{\mathrm{m}}, p_{\mathrm{s}} + p_{\mathrm{m}}, q_{\mathrm{s}} + q_{\mathrm{m}}) \tag{36}$$

and the parameter sequence

$$\mathcal{P}(r) = \left(\frac{r^{\nu}\eta k_{\mathrm{s}} k_{\mathrm{m}} c_{\mathrm{m}}}{E_{\mathrm{s}}/N_0}, \frac{r^{\nu}\eta c_{\mathrm{s}} c_{\mathrm{m}}^2}{E_{\mathrm{s}}/N_0}, \grave{\boldsymbol{a}}, \grave{\boldsymbol{b}}, \grave{\boldsymbol{\mathcal{A}}}, \grave{\boldsymbol{\mathcal{B}}}\right) \tag{37}$$

where

$$\grave{\boldsymbol{a}} = \left(\boldsymbol{a}_{\mathrm{s}}^{(1:n_{\mathrm{s}})}, \boldsymbol{a}_{\mathrm{m}}^{(1:n_{\mathrm{m}})} - \boldsymbol{\mathcal{A}}_{\mathrm{m}}^{(1:n_{\mathrm{m}})}, \boldsymbol{a}_{\mathrm{s}}^{(n_{\mathrm{s}}+1:p_{\mathrm{s}})}, \boldsymbol{a}_{\mathrm{m}}^{(n_{\mathrm{m}}+1:p_{\mathrm{m}})} - \boldsymbol{\mathcal{A}}_{\mathrm{m}}^{(n_{\mathrm{m}}+1:p_{\mathrm{m}})}\right) \tag{38}$$

$$\grave{\boldsymbol{b}} = \left(\boldsymbol{b}_{\mathrm{s}}^{(1:m_{\mathrm{s}})}, \boldsymbol{b}_{\mathrm{m}}^{(1:m_{\mathrm{m}})} - \boldsymbol{\mathcal{B}}_{\mathrm{m}}^{(1:m_{\mathrm{m}})}, \boldsymbol{b}_{\mathrm{s}}^{(m_{\mathrm{s}}+1:q_{\mathrm{s}})}, \boldsymbol{b}_{\mathrm{m}}^{(m_{\mathrm{m}}+1:q_{\mathrm{m}})} - \boldsymbol{\mathcal{B}}_{\mathrm{m}}^{(m_{\mathrm{m}}+1:q_{\mathrm{m}})}\right) \tag{39}$$

$$\grave{\boldsymbol{\mathcal{A}}} = \left(\boldsymbol{\mathcal{A}}_{\mathrm{s}}^{(1:n_{\mathrm{s}})}, 2\boldsymbol{\mathcal{A}}_{\mathrm{m}}^{(1:n_{\mathrm{m}})}, \boldsymbol{\mathcal{A}}_{\mathrm{s}}^{(n_{\mathrm{s}}+1:p_{\mathrm{s}})}, 2\boldsymbol{\mathcal{A}}_{\mathrm{m}}^{(n_{\mathrm{m}}+1:p_{\mathrm{m}})}\right) \tag{40}$$

$$\grave{\boldsymbol{\mathcal{B}}} = \left(\boldsymbol{\mathcal{B}}_{\mathrm{s}}^{(1:m_{\mathrm{s}})}, 2\boldsymbol{\mathcal{B}}_{\mathrm{m}}^{(1:m_{\mathrm{m}})}, \boldsymbol{\mathcal{B}}_{\mathrm{s}}^{(m_{\mathrm{s}}+1:q_{\mathrm{s}})}, 2\boldsymbol{\mathcal{B}}_{\mathrm{m}}^{(m_{\mathrm{m}}+1:q_{\mathrm{m}})}\right). \tag{41}$$

With spatial conditioning, the vehicle positions in the VANET are treated as deterministic and the VANET is viewed as a snapshot of a stationary random field of communicating vehicles.

Corollary 2 (Negative Binomial Vehicles): Let

$$\Lambda \sim \mathrm{Gamma}(\alpha_{\mathrm{v}}, \beta_{\mathrm{v}}) \tag{42}$$

$$X_\sigma \sim \mathcal{H}_{0,L}^{L,0}(\mathcal{P}_{\mathrm{s}} = (k_{\mathrm{s}}, c_{\mathrm{s}}, -, \boldsymbol{b}_{\mathrm{s}}, -, \boldsymbol{\mathcal{B}}_{\mathrm{s}})) \tag{43}$$

$$Z \sim \mathcal{H}_{0,M}^{M,0}(\mathcal{P}_{\mathrm{m}} = (k_{\mathrm{m}}, c_{\mathrm{m}}, -, \boldsymbol{b}_{\mathrm{m}}, -, \boldsymbol{\mathcal{B}}_{\mathrm{m}})). \tag{44}$$

$$\boldsymbol{a} = \left(\boldsymbol{a}_{\mathrm{s}}^{(1:n_{\mathrm{s}})}, \boldsymbol{a}_{\mathrm{m}}^{(1:n_{\mathrm{m}})} - \boldsymbol{\mathcal{A}}_{\mathrm{m}}^{(1:n_{\mathrm{m}})}, 1-\ell-\nu, \boldsymbol{a}_{\mathrm{v}}^{(1:n_{\mathrm{v}})} + (1-\nu)\,\boldsymbol{\mathcal{A}}_{\mathrm{v}}^{(1:n_{\mathrm{v}})}, \right.$$
$$\left. \boldsymbol{a}_{\mathrm{s}}^{(n_{\mathrm{s}}+1:p_{\mathrm{s}})}, \boldsymbol{a}_{\mathrm{m}}^{(n_{\mathrm{m}}+1:p_{\mathrm{m}})} - \boldsymbol{\mathcal{A}}_{\mathrm{m}}^{(n_{\mathrm{m}}+1:p_{\mathrm{m}})}, \boldsymbol{a}_{\mathrm{v}}^{(n_{\mathrm{v}}+1:p_{\mathrm{v}})} + (1-\nu)\,\boldsymbol{\mathcal{A}}_{\mathrm{v}}^{(n_{\mathrm{v}}+1:p_{\mathrm{v}})}\right) \quad (32)$$

$$\boldsymbol{b} = \left(\boldsymbol{b}_{\mathrm{s}}^{(1:m_{\mathrm{s}})}, \boldsymbol{b}_{\mathrm{m}}^{(1:m_{\mathrm{m}})} - \boldsymbol{\mathcal{B}}_{\mathrm{m}}^{(1:m_{\mathrm{m}})}, \boldsymbol{b}_{\mathrm{v}}^{(1:m_{\mathrm{v}})} + (1-\nu)\,\boldsymbol{\mathcal{B}}_{\mathrm{v}}^{(1:m_{\mathrm{v}})}, \right.$$
$$\left. \boldsymbol{b}_{\mathrm{s}}^{(m_{\mathrm{s}}+1:q_{\mathrm{s}})}, \boldsymbol{b}_{\mathrm{m}}^{(m_{\mathrm{m}}+1:q_{\mathrm{m}})} - \boldsymbol{\mathcal{B}}_{\mathrm{m}}^{(m_{\mathrm{m}}+1:q_{\mathrm{m}})}, \boldsymbol{b}_{\mathrm{v}}^{(m_{\mathrm{v}}+1:q_{\mathrm{v}})} + (1-\nu)\,\boldsymbol{\mathcal{B}}_{\mathrm{v}}^{(m_{\mathrm{v}}+1:q_{\mathrm{v}})}\right) \quad (33)$$

$$\boldsymbol{\mathcal{A}} = \left(\boldsymbol{\mathcal{A}}_{\mathrm{s}}^{(1:n_{\mathrm{s}})}, 2\boldsymbol{\mathcal{A}}_{\mathrm{m}}^{(1:n_{\mathrm{m}})}, \nu, \nu\boldsymbol{\mathcal{A}}_{\mathrm{v}}^{(1:n_{\mathrm{v}})}, \boldsymbol{\mathcal{A}}_{\mathrm{s}}^{(n_{\mathrm{s}}+1:p_{\mathrm{s}})}, 2\boldsymbol{\mathcal{A}}_{\mathrm{m}}^{(n_{\mathrm{m}}+1:p_{\mathrm{m}})}, \nu\boldsymbol{\mathcal{A}}_{\mathrm{v}}^{(n_{\mathrm{v}}+1:p_{\mathrm{v}})}\right) \quad (34)$$

$$\boldsymbol{\mathcal{B}} = \left(\boldsymbol{\mathcal{B}}_{\mathrm{s}}^{(1:m_{\mathrm{s}})}, 2\boldsymbol{\mathcal{B}}_{\mathrm{m}}^{(1:m_{\mathrm{m}})}, \nu\boldsymbol{\mathcal{B}}_{\mathrm{v}}^{(1:m_{\mathrm{v}})}, \boldsymbol{\mathcal{B}}_{\mathrm{s}}^{(m_{\mathrm{s}}+1:q_{\mathrm{s}})}, 2\boldsymbol{\mathcal{B}}_{\mathrm{m}}^{(m_{\mathrm{m}}+1:q_{\mathrm{m}})}, \nu\boldsymbol{\mathcal{B}}_{\mathrm{v}}^{(m_{\mathrm{v}}+1:q_{\mathrm{v}})}\right) \quad (35)$$

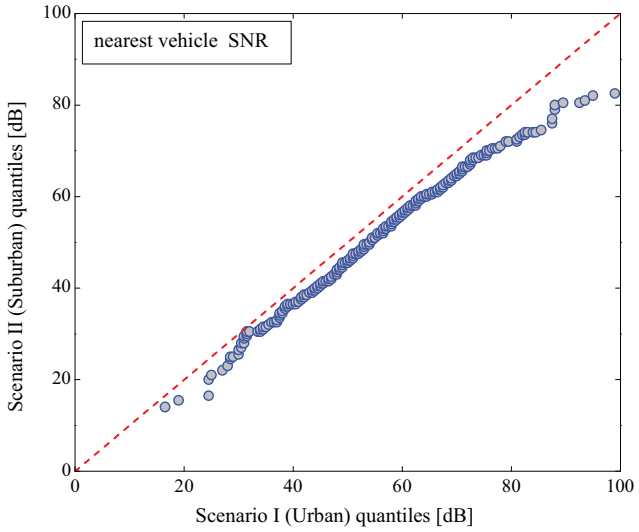

Fig. 8. Q-Q plot of the nearest vehicle's SNR γ_1 [dB] for Scenario I (Urban) and Scenario II (Suburban) when $E_{\mathrm{s}}/N_0 = 133.95$ dB (average transmit SNR).

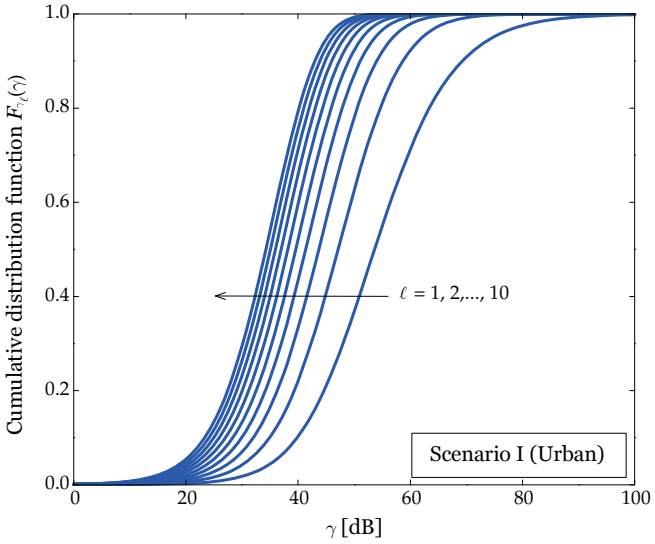

Fig. 9. CDF of the nearest vehicle's SNR γ_ℓ [dB] in Scenario I (Urban) for $\ell = 1, 2, \ldots, 10$ when $E_{\mathrm{s}}/N_0 = 133.95$ dB (average transmit SNR).

Then, we have Fox's H-SNR $\gamma_\ell \sim \mathcal{H}_{1,1+L+M}^{1+L+M,1}(\mathcal{P})$ with the parameter sequence

$$\mathcal{P} = \left(\frac{\eta k_{\mathrm{s}} k_{\mathrm{m}} c_{\mathrm{m}}}{E_{\mathrm{s}}/N_0 \beta_{\mathrm{v}}^{\nu} \Gamma(\alpha_{\mathrm{v}})\,(\ell-1)!}, \frac{\eta c_{\mathrm{s}} c_{\mathrm{m}}^2}{E_{\mathrm{s}}/N_0 \beta_{\mathrm{v}}^{\nu}}, 1-\ell-\nu, \right.$$
$$\left. (\boldsymbol{b}_{\mathrm{s}}, \boldsymbol{b}_{\mathrm{m}} - \boldsymbol{\mathcal{B}}_{\mathrm{m}}, \alpha_{\mathrm{v}} - \nu), \nu, (\boldsymbol{\mathcal{B}}_{\mathrm{s}}, 2\boldsymbol{\mathcal{B}}_{\mathrm{m}}, \nu)\right). \quad (45)$$

Proof: It follows from Corollary 1 and Theorem 2. □

Remark 4 (Poisson Vehicles): If $\beta_{\mathrm{v}} = \lambda_0/\alpha_{\mathrm{v}}$ and $\alpha_{\mathrm{v}} \to \infty$ in Corollary 2, then we have $R_\ell \sim \mathcal{H}_{0,1}^{1,0}(\mathcal{P}_{\mathrm{p}})$ (see Remark 2) and the instantaneous SNR at the ℓth nearest client vehicle in a Poisson field of vehicles reduces to $\gamma_\ell \sim \mathcal{H}_{1,L+M}^{L+M,1}(\mathcal{P})$ with the parameter sequence

$$\mathcal{P} = \left(\frac{\eta k_{\mathrm{s}} k_{\mathrm{m}} c_{\mathrm{m}}}{E_{\mathrm{s}}/N_0 \lambda_0^{\nu}\,(\ell-1)!}, \frac{\eta c_{\mathrm{s}} c_{\mathrm{m}}^2}{E_{\mathrm{s}}/N_0 \lambda_0^{\nu}}, 1-\ell-\nu, \right.$$
$$\left. (\boldsymbol{b}_{\mathrm{s}}, \boldsymbol{b}_{\mathrm{m}} - \boldsymbol{\mathcal{B}}_{\mathrm{m}}), \nu, (\boldsymbol{\mathcal{B}}_{\mathrm{s}}, 2\boldsymbol{\mathcal{B}}_{\mathrm{m}})\right). \quad (46)$$

Example 4 (Example Scenarios): To exemplify Cox–Fox modeling for intervehicle communication, we consider urban (Scenario I) and suburban (Scenario II) environments where V2V propagation characteristics (path loss, shadowing, and multipath fading) and spatial characteristics of vehicles are chosen as follows:

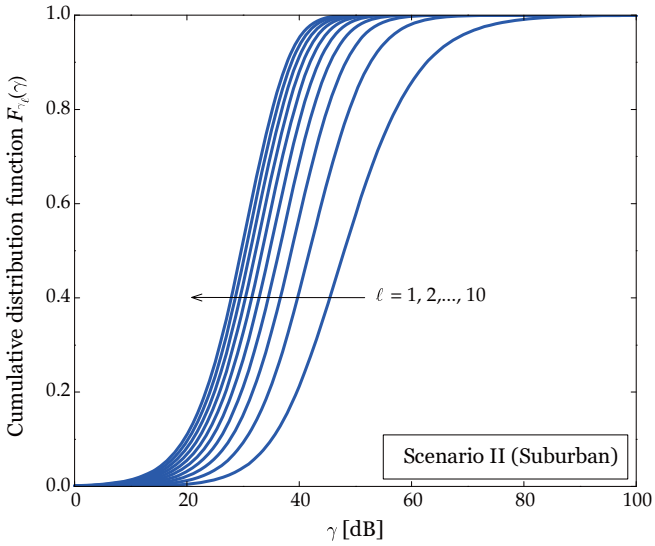

Fig. 10. CDF of the nearest vehicle's SNR γ_ℓ [dB] in Scenario II (Suburban) for $\ell = 1, 2, \ldots, 10$ when $E_{\mathrm{s}}/N_0 = 133.95$ dB (average transmit SNR).

- Scenario I (Urban): i) path loss/shadowing: Table II–Urban (Fox's H-fit); ii) multipath fading: Table IV–Measurement 1 (Fox's H-fit); and iii) vehicle spatial model: gamma Cox Ψ with $\Lambda \sim \mathrm{Gamma}(51.9354, 0.1770)$ vehicles/km. The ℓth nearest

TABLE V
PHYSICAL LAYER PARAMETERS (IEEE 802.11P PHY)

Parameter	Data rate (R_b)			
	3 Mbps	6 Mbps	12 Mbps	24 Mbps
Modulation	BPSK	QPSK	16-QAM	64-QAM
Symbol rate (R_s)	3 Msps	3 Msps	3 Msps	4 Msps
Average Tx power (P_av)	33 dBm	33 dBm	31.72 dBm	31.16 dBm
Maximum Tx power (P_tx)	33 dBm			
Noise PSD (N_0)	-167 dBm/Hz (-174 dBm/Hz + Noise figure 7 dB)			

client vehicle has the instantaneous SNR $\gamma_\ell \sim \mathcal{H}_{1,5}^{5,1}\left(\mathcal{P}_\mathrm{I}\right)$ with the parameter sequence

$$\mathcal{P}_\mathrm{I} = \left(\frac{3.44651\times 10^{-124}}{E_\mathrm{s}/N_0\,(\ell-1)!}, \frac{3.86\times 10^{17}}{E_\mathrm{s}/N_0}, -\ell-0.68, \right.$$
$$\left.(53.26, 1, -0.1, 4, 50.2554), 1.68, (3, \mathbf{1}_3, 1.68)\right). \tag{47}$$

- Scenario II (Suburban): i) path loss/shadowing: Table II–Suburban (Fox's H-fit); ii) multipath fading: Table IV–Measurement 2 (Fox's H-fit); and iii) vehicle spatial model: Poisson Ψ with $\lambda_0 = 6$ vehicles/km. The ℓth nearest client vehicle has the instantaneous SNR $\gamma_\ell \sim \mathcal{H}_{1,4}^{4,1}\left(\mathcal{P}_\mathrm{II}\right)$ with the parameter sequence

$$\mathcal{P}_\mathrm{II} = \left(\frac{1.65243\times 10^{-26}}{E_\mathrm{s}/N_0\,(\ell-1)!}, \frac{1.77121\times 10^{14}}{E_\mathrm{s}/N_0}, -\ell-0.59, \right.$$
$$\left.(33.03, -0.05, 1.5, 1.6), 1.59, (3, \mathbf{1}_2, 0.4)\right). \tag{48}$$

In both the scenarios, we use physical layer parameters in IEEE 802.11p PHY (see Table V). Fig. 8 shows the Q-Q plot of the nearest vehicle's SNR γ_1 for Scenario I (Urban) and Scenario II (Suburban) when $E_\mathrm{s}/N_0 = 133.95$ dB, which is equal to the average transmit SNR for 16-ary quadrature amplitude modulation (16-QAM).[9] Since the Q-Q plot has the similar slope with the reference red dashed line, two SNR distributions for Scenarios I and II have reasonably similar shapes. Since the Q-Q plot lies below the reference, the nearest vehicle SNR γ_1 for Scenario I is supposed to be better than γ_1 for Scenario II. To further ascertain the SNR characteristics, the CDFs $F_{\gamma_\ell}(\gamma)$ of the ℓth nearest vehicle's SNR γ_ℓ are depicted in Figs. 9 and 10 for $\ell = 1, 2, \ldots, 10$ in Scenarios I and II, respectively. In these figures, we also observe that Scenario I has slightly better SNR characteristics than Scenario II.

IV. ERROR PROBABILITY AND CHANNEL CAPACITY

Using the Cox–Fox model in Theorem 2, we now establish a unifying framework to analyze two fundamental physical-layer performances (i.e., error probability and channel capacity) for intervehicle communication in a Cox field of vehicles, where

[9]The transmit SNR of 133.95 dB corresponds to the average received SNR of 47.56 dB for Scenario I and 45.57 dB for Scenario II at the 200-meter distance from the transmitter.

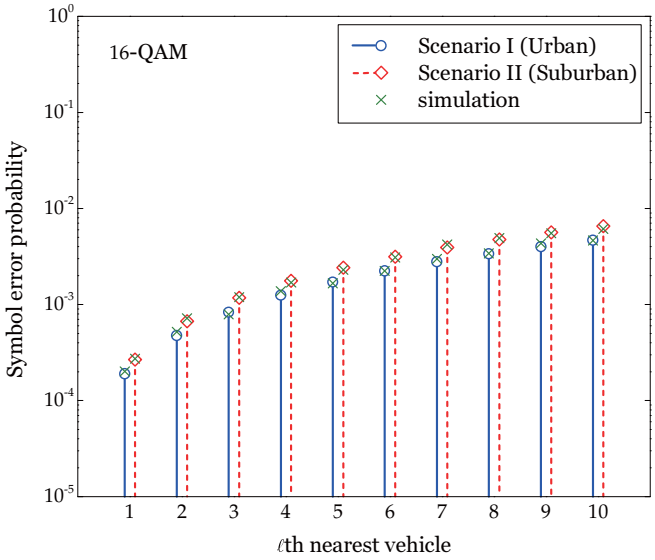

Fig. 11. Average SEP $P_{\mathrm{e},\ell}$ for 16-QAM at the ℓth nearest client vehicle in Scenario I (Urban) and Scenario II (Suburban) for $\ell = 1, 2, \ldots, 10$.

the ℓth nearest client vehicle in the cluster $\mathcal{V}$ has Fox's H-SNR $\gamma_\ell \sim \mathcal{H}_{p,q}^{m,n}\left(\mathcal{P}\right)$ stated in Theorem 2.

A. Error Probability

For two-dimensional signaling constellation with polygonal decision boundaries, the average SEP for coherent detection at the ℓth nearest client vehicle can be written as

$$P_{\mathrm{e},\ell} \triangleq \mathbb{E}_{Z,X_\sigma,R_\ell}\left\{\mathbb{P}\left\{\mathrm{error}\middle|Z, X_\sigma, R_\ell\right\}\right\}$$
$$= \sum_{i=1}^{M} p_i \sum_{j\in\mathcal{B}_i} \frac{1}{2\pi}\int_0^{\Theta_{ij}} \phi_{\gamma_\ell}\left(\frac{w_{ij}}{4\sin^2\left(\theta+\varphi_{ij}\right)}\right) d\theta \tag{49}$$

where M is the constellation size; $\{p_i\}_{i=1}^{M}$ are the *a priori* symbol probabilities; and φ_{ij}, w_{ij}, Θ_{ij}, and $\mathcal{B}_i$ are the quantities depending on the geometry of the constellation [44]–[47].

Theorem 3 (Average SEP): Let $\gamma_\ell \sim \mathcal{H}_{p,q}^{m,n}\left(\mathcal{P}\right)$ be the instantaneous SNR at the ℓth nearest client vehicle. Then, the average SEP for coherent detection of two-dimensional signals at the ℓth nearest client vehicle is given by

$$P_{\mathrm{e},\ell} = \sum_{i=1}^{M} p_i \sum_{j\in\mathcal{B}_i}\left\{\mathcal{I}_{\varphi_{ij}}(w_{ij}) + \mathcal{I}_{\pi-\Theta_{ij}-\varphi_{ij}}(w_{ij})\right\} \tag{50}$$

$$\mathcal{I}_{\varphi}\left(w\right)=\begin{cases} H_{p+2,q+1}^{m,n+2}\left(\dfrac{1}{w};\mathcal{P}_{\text{sep}}=\left(\dfrac{\mathcal{k}}{4c\sqrt{\pi}},4c,\left(\frac{1}{2},1,\boldsymbol{a}+\boldsymbol{\mathcal{A}}\right),\left(\boldsymbol{b}+\boldsymbol{\mathcal{B}},0\right),\left(\mathbf{1}_2,\boldsymbol{\mathcal{A}}\right),\left(\boldsymbol{\mathcal{B}},1\right)\right)\right), & \text{if } \varphi=0 \\ \dfrac{\mathcal{k}\cos\varphi}{4\pi c}H_{1,(q:1),0,(p+2,2)}^{1,m,1,n+1,1}\left[\begin{array}{c|l} \dfrac{w}{4c} & \left(\frac{1}{2},1\right) \\ -\cos^2\varphi & \left(u_1,\mathcal{B}_1\right),\ldots,\left(u_q,\mathcal{B}_q\right);\left(-\frac{1}{2},1\right) \\ & \text{—} \\ & \left(0,1\right),\left(v_1,\mathcal{A}_1\right),\ldots,\left(v_p,\mathcal{A}_p\right),\left(-\frac{1}{2},1\right);\left(0,1\right),\left(-\frac{1}{2},1\right) \end{array}\right], & \text{if } \varphi\in\left(0,\tfrac{\pi}{2}\right] \end{cases} \tag{52}$$

$$\begin{aligned} \mathcal{I}_0\left(w\right) &= \frac{\mathcal{k}}{4\pi c}\int_0^1 \frac{1}{\sqrt{x\left(1-x\right)}}H_{p+1,q}^{m,n+1}\left[\frac{4c}{w}\left(1-x\right)\middle|\begin{array}{l}\left(1,1\right),\left(a_1+\mathcal{A}_1,\mathcal{A}_1\right),\ldots,\left(a_p+\mathcal{A}_p,\mathcal{A}_p\right)\\ \left(b_1+\mathcal{B}_1,\mathcal{B}_1\right),\ldots,\left(b_q+\mathcal{B}_q,\mathcal{B}_q\right)\end{array}\right]dx \\ &\overset{(a)}{=} \frac{\mathcal{k}}{4\pi c}H_{p+3,q+1}^{m,n+3}\left[\frac{4c}{w}\middle|\begin{array}{l}\left(\frac{1}{2},0\right),\left(\frac{1}{2},1\right),\left(1,1\right),\left(a_1+\mathcal{A}_1,\mathcal{A}_1\right),\ldots,\left(a_p+\mathcal{A}_p,\mathcal{A}_p\right)\\ \left(b_1+\mathcal{B}_1,\mathcal{B}_1\right),\ldots,\left(b_q+\mathcal{B}_q,\mathcal{B}_q\right),\left(0,1\right)\end{array}\right] \\ &\overset{(b)}{=} \frac{\mathcal{k}}{4\sqrt{\pi}c}H_{p+2,q+1}^{m,n+2}\left[\frac{4c}{w}\middle|\begin{array}{l}\left(\frac{1}{2},1\right),\left(1,1\right),\left(a_1+\mathcal{A}_1,\mathcal{A}_1\right),\ldots,\left(a_p+\mathcal{A}_p,\mathcal{A}_p\right)\\ \left(b_1+\mathcal{B}_1,\mathcal{B}_1\right),\ldots,\left(b_q+\mathcal{B}_q,\mathcal{B}_q\right),\left(0,1\right)\end{array}\right] \end{aligned} \tag{53}$$

$$\mathcal{I}_{\varphi}\left(w\right)=\frac{\mathcal{k}\cos\varphi}{4\pi c}\int_0^1 \frac{1}{\sqrt{x\left(1-x\cos^2\varphi\right)}}H_{p+1,q}^{m,n+1}\left[\frac{4c}{w}\left(1-x\cos^2\varphi\right)\middle|\begin{array}{l}\left(1,1\right),\left(a_1+\mathcal{A}_1,\mathcal{A}_1\right),\ldots,\left(a_p+\mathcal{A}_p,\mathcal{A}_p\right)\\ \left(b_1+\mathcal{B}_1,\mathcal{B}_1\right),\ldots,\left(b_q+\mathcal{B}_q,\mathcal{B}_q\right)\end{array}\right]dx \tag{54}$$

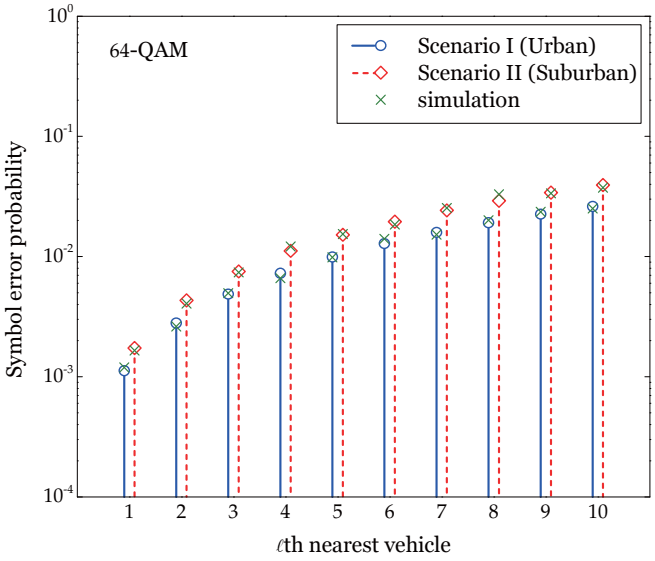

Fig. 12. Average SEP $P_{\mathrm{e},\ell}$ for 64-QAM at the ℓth nearest client vehicle in Scenario I (Urban) and Scenario II (Suburban) for $\ell=1,2,\ldots,10$.

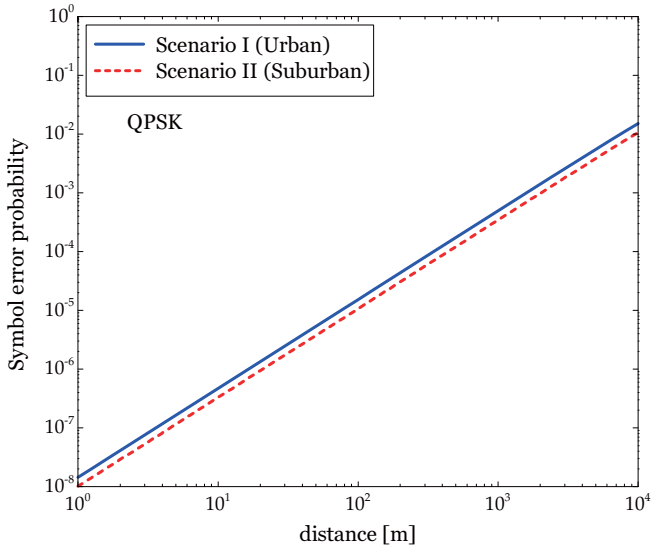

Fig. 13. Average SEP for QPSK as a function of the vehicle distance r for Scenario I (Urban) and Scenario II (Suburban). In this spatial conditioning example, the location-conditioned SNR $\gamma_\ell\left(r\right)\overset{|R}{\sim}\mathcal{H}_{p,q}^{m,n}\left(\mathcal{P}\left(r\right)\right)$ in Remark 3 is used instead for each scenario.

where $\mathcal{I}_{\varphi}\left(w\right)$ is defined as

$$\mathcal{I}_{\varphi}\left(w\right)\triangleq\frac{1}{2\pi}\int_{\varphi}^{\pi/2}\phi_{\gamma_\ell}\left(\frac{w}{4\sin^2\theta}\right)d\theta,\quad 0\le\varphi\le\frac{\pi}{2} \tag{51}$$

which has the closed-form solution (52), where $u_i=1-b_i-\mathcal{B}_i$ and $v_j=1-a_j-\mathcal{A}_j$.

Proof: It follows from (49), (51), and the fact that $\pi/2\le\Theta_{ij}+\varphi_{ij}\le\pi$. Using Property 2, we obtain the closed-form solution for $\mathcal{I}_{\varphi}\left(w\right)$ as follows:

i) Case $\varphi=0$: Making the change of variable $x=\cos^2\theta$, we get (53), where (a) and (b) follow from [33, eq. (2.25.2.2)] and [31, eq. (1.65)], respectively.

ii) Case $\varphi\in(0,\pi/2]$: Making the change of variable $x=\cos^2\theta/\cos^2\varphi$, we get (54). Using the fractional integration of Fox's H-function [31, eq. (2.69)], we arrive at the desired result.

□

Remark 5: The average SEP $P_{\mathrm{e},\ell}$ measures the communication reliability at the ℓth nearest client vehicle by averaging both small- and large-scale fading processes (Z and X_σ) in time and random (distance-dependent) path losses (R^{ν}) in space. Given $R_\ell=r$ (spatial conditioning), the location-conditioned average SEP can be obtained using instead $\gamma_\ell\left(r\right)\overset{|R}{\sim}\mathcal{H}_{p,q}^{m,n}\left(\mathcal{P}\left(r\right)\right)$ in Remark 3.

Example 5 (M-PSK and M-QAM): The SEP (49) reduces to the well-known expressions for equiprobable M-ary phase-

$$\begin{aligned} P_{\mathrm{e},\ell} &\doteq H_{q,p+1}^{n+1,m}\left[E_{\mathrm{s}}/N_0 \,\middle|\, \begin{matrix}(1-\mathcal{b}_1-\mathcal{B}_1,\mathcal{B}_1),\ldots,(1-\mathcal{b}_q-\mathcal{B}_q,\mathcal{B}_q)\\ (0,1),(1-a_1-\mathcal{A}_1,\mathcal{A}_1),\ldots,(1-a_p-\mathcal{A}_p,\mathcal{A}_p)\end{matrix}\right] \\ &\doteq H_{p+1,q}^{m,n+1}\left[(E_{\mathrm{s}}/N_0)^{-1} \,\middle|\, \begin{matrix}(1,1),(a_1+\mathcal{A}_1,\mathcal{A}_1),\ldots,(a_p+\mathcal{A}_p,\mathcal{A}_p)\\ (\mathcal{b}_1+\mathcal{B}_1,\mathcal{B}_1),\ldots,(\mathcal{b}_q+\mathcal{B}_q,\mathcal{B}_q)\end{matrix}\right] \\ &\doteq (E_{\mathrm{s}}/N_0)^{-\min_{1\le j\le m}\left[1+\frac{\Re\mathfrak{e}\,\mathcal{b}_j}{\mathcal{B}_j}\right]} \end{aligned} \tag{60}$$

$$\mathcal{P}_{\mathrm{ec}} = \left(\frac{\mathcal{k}}{\ln 2}, c, \left(\boldsymbol{a}^{(1:n)}, -1, 0, \boldsymbol{a}^{(n+1:p)}\right), \left(\boldsymbol{\mathcal{b}}^{(1:m)}, -\mathbf{1}_2, \boldsymbol{\mathcal{b}}^{(m+1:q)}\right), \left(\boldsymbol{\mathcal{A}}^{(1:n)}, \mathbf{1}_2, \boldsymbol{\mathcal{A}}^{(n+1:p)}\right), \left(\boldsymbol{\mathcal{B}}^{(1:m)}, \mathbf{1}_2, \boldsymbol{\mathcal{B}}^{(m+1:q)}\right)\right) \tag{63}$$

$$\begin{aligned} \langle C\rangle_\ell &= \int_0^\infty H_{p,q}^{m,n}(x;\mathcal{P})\, H_{2,2}^{1,2}\left(x;\left(\frac{1}{\ln 2},1,\mathbf{1}_2,(1,0),\mathbf{1}_2,\mathbf{1}_2\right)\right)dx \\ &= \frac{\mathcal{k}}{\ln 2} H_{p+2,q+2}^{m+2,n+1}\left[c \,\middle|\, \begin{matrix}(a_1,\mathcal{A}_1),\ldots,(a_n,\mathcal{A}_n),(-1,1),(0,1),(a_{n+1},\mathcal{A}_{n+1}),\ldots,(a_p,\mathcal{A}_p)\\ (\mathcal{b}_1,\mathcal{B}_1),\ldots,(\mathcal{b}_m,\mathcal{B}_m),(-1,1),(-1,1),(\mathcal{b}_{m+1},\mathcal{B}_{m+1}),\ldots,(\mathcal{b}_q,\mathcal{B}_q)\end{matrix}\right] \end{aligned} \tag{64}$$

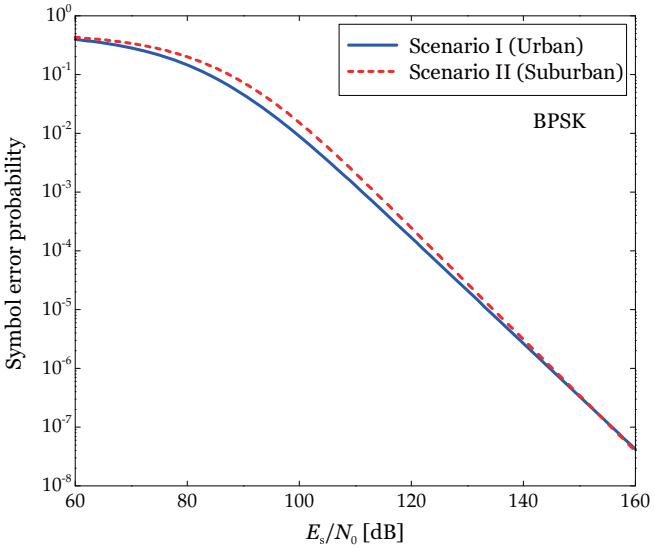

Fig. 14. Average SEP $P_{\mathrm{e},1}$ for BPSK at the nearest client vehicle as a function of the average transmit SNR E_{s}/N_0 in Scenario I (Urban) and Scenario II (Suburban).

shift keying (M-PSK) and M-QAM signals as in [48, eqs. (9) and (11)], respectively. Hence, we have

$$P_{\mathrm{e},\ell}^{\mathrm{MPSK}} = 2\mathcal{I}_0\left(4g_{\mathrm{MPSK}}\right) + 2\mathcal{I}_{\pi/M}\left(4g_{\mathrm{MPSK}}\right) \tag{55}$$

$$\begin{aligned} P_{\mathrm{e},\ell}^{\mathrm{MQAM}} &= \frac{8}{\sqrt{M}}\left(1-\frac{1}{\sqrt{M}}\right)\mathcal{I}_0\left(4g_{\mathrm{MQAM}}\right) \\ &\quad + 8\left(1-\frac{1}{\sqrt{M}}\right)^2 \mathcal{I}_{\pi/4}\left(4g_{\mathrm{MQAM}}\right) \end{aligned} \tag{56}$$

where $g_{\mathrm{MPSK}} = \sin^2(\pi/M)$ and $g_{\mathrm{MQAM}} = \frac{3}{2(M-1)}$. Figs. 11 and 12 show the average SEPs $P_{\mathrm{e},\ell}$ for 16-QAM and 64-QAM at the ℓth nearest client vehicle in Scenarios I and II for $\ell = 1, 2, \ldots, 10$. We observe that the simulation results agree exactly with the analytical results and Scenario I has lower SEP values than Scenario II due to the better SNR characteristics. The average SEP for QPSK is also depicted in Fig. 13 as a function of the vehicle distance r for two scenarios, where the location-conditioned SNR $\gamma_\ell(r) \overset{|R}{\sim} \mathcal{H}_{p,q}^{m,n}(\mathcal{P}(r))$ in Remark 3 is used instead for each scenario.

We further characterize the high-SNR behavior of the average SEP in terms of its H-parameters in the following theorem.

Corollary 3 (High-SNR Slope): Let

$$\zeta_\ell \triangleq \lim_{E_{\mathrm{s}}/N_0\to\infty} \frac{-\log P_{\mathrm{e},\ell}}{\log E_{\mathrm{s}}/N_0} \tag{57}$$

be the high-SNR slope of the SEP $P_{\mathrm{e},\ell}$ at the ℓth nearest client vehicle. Then, we have

$$\zeta_\ell = \min_{1\le j\le m}\left[1+\frac{\Re\mathfrak{e}\,\mathcal{b}_j}{\mathcal{B}_j}\right]. \tag{58}$$

Proof: As E_{s}/N_0 goes to infinity, we have $P_{\mathrm{e},\ell} \doteq \phi_{\gamma_\ell}(1)$ [49]. Using the asymptotic expansion of Fox's H-function [31, Theorem 1.2]

$$H_{p,q}^{m,n}\left(x^{-1};\mathcal{P}\right) \doteq x^{-\min_{1\le j\le m}\left[\frac{\Re\mathfrak{e}\,\mathcal{b}_j}{\mathcal{B}_j}\right]} \tag{59}$$

(where $\sum_{j=1}^q \mathcal{B}_j \ge \sum_{j=1}^p \mathcal{A}_j$), we have (60), which completes the proof. □

Remark 6: Corollary 3 states that the high-SNR slope of the SEP $P_{\mathrm{e},\ell}$ is only a function of the pass loss exponent ν, $\mathcal{b}$-, and $\mathcal{B}$-parameters of vehicle concentration, shadowing, and multipath fading H-variates, while not depending on the spatial order index ℓ.

Example 6: In Scenario I, the ℓth nearest client vehicle has the instantaneous SNR $\gamma_\ell \sim \mathcal{H}_{1,5}^{5,1}(\mathcal{P}_{\mathrm{I}})$ with the parameter sequence $\mathcal{P}_{\mathrm{I}}$ in (47). In this case, the high-SNR slope is equal to $\zeta_\ell = 0.9$ determined by the parameters $\mathcal{b}_3 = -0.1$ and $\mathcal{B}_3 = 1$. In Scenario II, we have $\gamma_\ell \sim \mathcal{H}_{1,4}^{4,1}(\mathcal{P}_{\mathrm{II}})$ with the parameter sequence $\mathcal{P}_{\mathrm{II}}$ in (48), leading to the high-SNR slope equal to $\zeta_\ell = 0.95$. In both scenarios, the V2V channels are worse than Rayleigh fading where the slope is equal to 1. The role of Fox's H-parameters ($\mathcal{b}$'s and $\mathcal{B}$'s) on the high-SNR SEP slope is akin to multipath scattering or clustering of cascaded wireless channels such as keyhole, double scattering, and multiple-antenna relay channels [49]–[52], where the worst diversity link governs the overall channel diversity capability. To ascertain the high-SNR SEP behavior, the average SEP $P_{\mathrm{e},1}$ for BPSK at the nearest client vehicle is depicted in Fig. 14 as

a function of E_s/N_0 in Scenarios I and II. In this figure, we observe that the high-SNR slope (ζ_1 =0.95) for Scenario II is slightly larger than the slope (ζ_1 =0.9) for Scenario I.

B. Channel Capacity

Theorem 4 (Ergodic Capacity): Let

$$\langle C\rangle_\ell \triangleq \mathbb{E}\left\{\log_2\left(1+\gamma_\ell\right)\right\} \tag{61}$$

be the ergodic capacity [bits/s/Hz] of a communication link between the beacon vehicle and the ℓth nearest client vehicle. Then, we have

$$\langle C\rangle_\ell = H_{p+2,q+2}^{m+2,n+1}\left(1;\mathcal{P}_{\mathsf{ec}}\right) \tag{62}$$

where the parameter sequence $\mathcal{P}_{\mathsf{ec}}$ is given by (63).

Proof: Expressing $\log_2(1+x)$ in terms of Fox's H-function with the help of [33, eq. (8.4.6.5)] and using the Mellin transform of the product of two Fox's H-functions [33, eq. (2.25.1.1)], we get (64), which complete the proof. □

Theorem 5 (Outage Capacity): Let

$$C_{\mathrm{out},\ell}(\epsilon) \triangleq \sup_{R\geq 0}\left\{R:\mathbb{P}\left\{\log_2\left(1+\gamma_\ell\right)\leq R\right\}\leq\epsilon\right\} \tag{65}$$

be the outage capacity (bits/s/Hz) at outage probability ϵ of the ℓth nearest link. Then, the outage capacity $C_{\mathrm{out},\ell}(\epsilon)$ is the solution of

$$H_{p+1,q+1}^{m+1,n}\left(2^{C_{\mathrm{out},\ell}(\epsilon)}-1;\mathcal{P}_{\mathsf{cdf}}\right)=1-\epsilon. \tag{66}$$

Proof: It follows readily from Property 1 and the fact that $F_{\gamma_\ell}\left(2^{C_{\mathrm{out},\ell}(\epsilon)}-1\right)=\epsilon$. □

Example 7: Fig. 15 shows the ergodic capacity $\langle C\rangle_\ell$ of the ℓth nearest client vehicle in Scenarios I and II for $\ell=1,2,\ldots,10$ when E_s/N_0 = 133.95 dB. We observe again that the simulation results agree with the analytical results. The ergodic capacity is also depicted in Fig. 16 as a function of the vehicle distance r for two scenarios. In this figure, the location-conditioned SNR $\gamma_\ell(r)\overset{|R}{\sim}\mathcal{H}_{p,q}^{m,n}\left(\mathcal{P}(r)\right)$ in Remark 3 is used instead for each scenario. Since the path loss exponent for Scenario I is slightly larger than the exponent for Scenario II, the capacity gap between two scenarios decreases at a large distance in this spatial conditioning example.

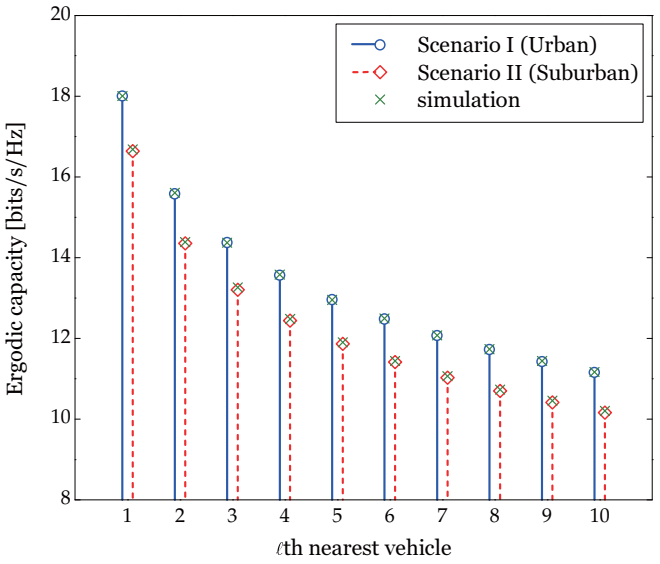

Fig. 15. Ergodic capacity $\langle C\rangle_\ell$ of the ℓth nearest client vehicle in Scenario I (Urban) and Scenario II (Suburban) for $\ell=1,2,\ldots,10$ when E_s/N_0 = 133.95 dB (average transmit SNR).

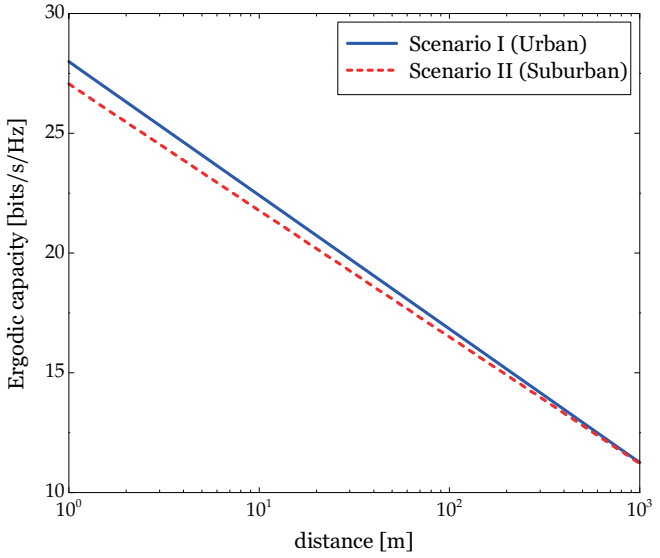

Fig. 16. Ergodic capacity as a function of the vehicle distance r for Scenario I (Urban) and Scenario II (Suburban) when E_s/N_0 = 133.95 dB (average transmit SNR). In this spatial conditioning example, the location-conditioned SNR $\gamma_\ell(r)\overset{|R}{\sim}\mathcal{H}_{p,q}^{m,n}\left(\mathcal{P}(r)\right)$ in Remark 3 is used instead for each scenario.

V. Conclusion

Using general forms—namely, Cox process and Fox's H-variate—of point processes and stochastic variables, we developed the unifying Cox–Fox framework to characterize V2V communication in a doubly stochastic VANET by *spatio-temporally* averaging the path loss, shadowing, and multipath fading effects. In this framework, individual propagation characteristics are first modeled as versatile Fox's H-variates and then integrated into a single compound Fox's H-variate using the H-preserving property under products, powers, quotients, and their combinations. The Cox–Fox model can encompass a large number of well-known or generalized statistical propagation models; enable accurate fits to measurement data by varying parameters; and establish a unified analysis for error probability and channel capacity in terms of again Fox's H-functions. This new methodology is also applicable to a variety of wireless networks, each with unique wireless propagation and spatial characterizations, such as wireless local area networks, cellular networks, ad-hoc sensor networks, relay networks, cognitive radio networks, and femtocell networks.

References

[1] *Wireless LAN Medium Access Control (MAC) and Physical Layer (PHY) Specifications—Amendment 6: Wireless Access in Vehicular Environments*, IEEE Standard 802.11p, July 2010.

[2] *Wireless LAN Medium Access Control (MAC) and Physical Layer (PHY) Specifications: High-speed Physical Layer in the 5 GHz Band*, IEEE Standard 802.11a, Sep. 1999.

[3] *IEEE Trial-Use Standard for Wireless Access in Vehicular Environments (WAVE)—Resource Manager*, IEEE Standard 1609.1, Oct. 2006.

[4] L. Cheng, B. E. Henty, D. D. Stancil, F. Bai, and P. Mudalige, "Mobile vehicle-to-vehicle narrow-band channel measurement and characterization of the 5.9 GHz dedicated short range communication (DSRC)

frequency band," *IEEE J. Sel. Areas Commun.*, vol. 25, no. 8, pp. 1501–1516, Oct. 2007.
[5] A. Paier, J. Karedal, N. Czink, C. Dumard, T. Zemen, F. Tufvesson, A. F. Molisch, and C. F. Mecklenbrauker, "Characterization of vehicle-to-vehicle radio channels from measurement at 5.2 GHz," *Wireless Pers. Commun.*, vol. 25, pp. 19–29, 2009.
[6] J. Karedal, N. Czink, A. Paier, F. Tufvesson, and A. F. Molisch, "Path loss modeling for vehicle-to-vehicle communications," *IEEE Trans. Veh. Technol.*, vol. 60, no. 1, pp. 323–328, Jan. 2011.
[7] C. F. Mecklenbrauker, A. F. Molisch, J. Karedal, F. Tufvesson, A. Paier, L. Bernadó, T. Zemen, O. Klemp, and N. Czink, "Vehicular channel characterization and its implications for wireless system design and performance," *Proc. IEEE*, vol. 99, no. 7, pp. 1189–1212, July 2011.
[8] M. Bohan, T. T. V. Vinhoza, M. Ferreira, J. Barros, and O. K. Tonguz, "Impact of vehicles as obstacles in vehicular ad hoc networks," *IEEE J. Sel. Areas Commun.*, vol. 29, no. 1, pp. 15–28, Jan. 2011.
[9] C.-X. Wang, X. Cheng, and D. I. Laurenson, "Vehicle-to-vehicle channel modeling and measurements: Recent advances and future challenges," *IEEE Commun. Mag.*, vol. 47, no. 11, pp. 96–103, Nov. 2009.
[10] D. W. Matolak and J. Frolik, "Worse-than-Rayleigh fading: Experimental results and theoretical models," *IEEE Commun. Mag.*, vol. 49, no. 4, pp. 140–146, Apr. 2011.
[11] I. Sen and D. W. Matolak, "Vehicle-vehicle channel models for the 5-GHz band," *IEEE Trans. Intell. Transp. Syst.*, vol. 9, no. 2, pp. 235–245, June 2008.
[12] Q. Wu, D. W. Matolak, and I. Sen, "5-GHz-band vehicle-to-vehicle channels: Models for multiple values of channel bandwidth," *IEEE Trans. Veh. Technol.*, vol. 59, no. 5, pp. 2620–2625, June 2010.
[13] J. G. Wardrop, "Some theoretical aspects of road traffic research," *Road Eng. Division Meeting*, pp. 325–362, Jan. 1952.
[14] H. Greenberg, "An analysis of traffic flow," *Operations Research*, vol. 7, no. 1, pp. 79–85, Jan.–Feb. 1959.
[15] D. Chowdhury, L. Santen, and A. Schadschneider, "Statistical physics of vehicular traffic and some related systems," *Physics Reports 329*, pp. 199–329, 2000.
[16] D. Helbing, "Traffic and related self-driven many-particle systems," *Reviews Modern Physics*, vol. 73, no. 4, pp. 1067–1141, Oct. 2001.
[17] D. L. Gerlough and M. J. Huber, *Traffic Flow Theory: A Monograph*. Washington, DC: Transportation Research Board National Research Council, 1975.
[18] D. Stoyan, W. Kendall, and J. Mecke, *Stochastic Geometry and Its Applications*, 2nd ed. John Wiley and Sons, 1996.
[19] D. R. Cox, "Some statistical methods connected with series of events," *J. Royal Statistical Soc.*, vol. 17, no. 2, pp. 129–164, 1955.
[20] D. R. Cox and V. Isham, *Point Processes*. London and New York: Chapman and Hall, 1980.
[21] J. Orriss and S. K. Barton, "Probability distributions for the number of radio transceivers which can communicate with one another," *IEEE Trans. Commun.*, vol. 51, no. 4, pp. 676–681, Apr. 2003.
[22] M. Z. Win, "A mathematical model for network interference," in *Proc. IEEE Commun. Theory Workshop*, May 2007.
[23] M. Z. Win, P. C. Pinto, and L. A. Shepp, "A mathematical theory of network interference and its applications," *Proc. IEEE*, vol. 97, no. 2, pp. 205–230, Feb. 2009.
[24] E. Salbaroli and A. Zanella, "Interference analysis in a Poisson field of nodes of finite area," *IEEE Trans. Veh. Technol.*, vol. 58, no. 4, pp. 1776–1783, May 2009.
[25] K. Huang, V. K. N. Lau, and Y. Chen, "Spectrum sharing between cellular and mobile ad hoc networks: Transmission-capacity trade-off," *IEEE J. Sel. Areas Commun.*, vol. 27, no. 7, pp. 1256–1267, Sep. 2009.
[26] M. Haenggi, J. G. Andrews, F. Baccelli, O. Dousse, and M. Franceschetti, "Stochastic geometry and random graphs for the analysis and design of wireless networks," *IEEE J. Sel. Areas Commun.*, vol. 27, no. 7, pp. 1029–1046, Sep. 2009.
[27] B. D. Carter and M. D. Springer, "The distribution of products, quotients and powers of independent H-function variates," *SIAM J. Applied Mathematics*, vol. 33, no. 4, pp. 542–558, Dec. 1977.
[28] C. Fox, "The G and H-functions as symmetrical Fourier kernels," *Trans. Amer. Math. Soc.*, vol. 98, pp. 395–429, 1961.
[29] A. M. Mathai and R. K. Saxena, *The H-Function with Applications in Statistics and Other Disciplines*. New York: Wiley, 1978.
[30] A. A. Kilbas and M. Saigo, *H-Transform: Theory and Applications*. Boca Raton, FL: CRC Press LLC, 2004.
[31] A. M. Mathai, R. K. Saxena, and H. J. Haubold, *The H-Function: Theory and Applications*. New York: Springer, 2010.
[32] I. S. Gradshteyn and I. M. Ryzhik, *Table of Integrals, Series, and Products*, 7th ed. San Diego, CA: Academic, 2007.
[33] A. P. Prudnikov, Y. A. Brychkov, and O. I. Marichev, *Integrals and Series*. New York: Gordon and Breach Science, 1990, vol. 3.
[34] M. Greenwood and G. U. Yule, "An inquiry into the nature of frequency distributions representative of multiple happenings with particular reference to the occurrence of multiple attacks of disease or of repeated accidents," *J. Royal Statistical Soc.*, vol. 83, no. 2, pp. 255–279, Mar. 1920.
[35] O. Barndorff-Nielsen and G. F. Yeo, "Negative binomial processes," *J. Applied Probability*, vol. 6, no. 3, pp. 633–647, Dec. 1969.
[36] A. Abdi and M. Kaveh, "K distribution: An appropriate substitute for Rayleigh-lognormal distribution in fading-shadowing wireless channels," *Electon. Lett.*, vol. 34, no. 9, pp. 851–852, Apr. 1998.
[37] I. M. Kostiè, "Analytical approach to performance analysis for channel subject to shadowing and fading," *IEE Proc. Commun.*, vol. 152, no. 6, pp. 821–827, Dec. 2005.
[38] M. D. Yacoub, "The α-μ distribution: A physical fading model for the Stacy distribution," *IEEE Trans. Veh. Technol.*, vol. 56, no. 1, pp. 27–34, Jan. 2007.
[39] Y. Song, H. Shin, and W. Kim, "Asymptotic SEP for M-PSK signals over α-μ fading channels," *IEEE Commun. Lett.*, vol. 12, no. 9, pp. 675–677, Sep. 2008.
[40] Y. Song and H. Shin, "Symbol error probability for M-ary signals in Stacy fading channels," *IEICE Trans. Commun.*, vol. E92-B, no. 3, pp. 973–979, Mar. 2009.
[41] Y. Jeong, J. W. Chong, and H. Shin, "Ergodic capacity of X-μ fading channels," in *Proc. IEEE VTS Asia Pacific Wireless Commun. Symp. (APWCS)*, May 2010, pp. 1–5.
[42] G. K. Karagiannidis, N. C. Sagias, and P. T. Mathiopoulos, "N*Nakagami: A novel stochastic model for cascaded fading channels," *IEEE Trans. Commun.*, vol. 55, no. 8, pp. 1453–1458, Aug. 2007.
[43] H. İlhan, M. Uysal, and I. Altunbaş, "Cooperative diversity for intervehicular communication: Performance analysis and optimization," *IEEE Trans. Veh. Technol.*, vol. 58, no. 7, pp. 3301–3310, Sep. 2009.
[44] W. M. Gifford, M. Z. Win, and M. Chiani, "Antenna subset diversity with non-ideal channel estimation," *IEEE Trans. Wireless Commun.*, vol. 7, no. 5, pp. 1527–1539, May 2008.
[45] A. Conti, W. M. Gifford, M. Z. Win, and M. Chiani, "Optimized simple bounds for diversity systems," *IEEE Trans. Commun.*, vol. 57, no. 9, pp. 2674–2685, Sep. 2009.
[46] Y. Jeong, H. Shin, and M. Z. Win, "Superanalysis of optimum combining with application to femtocell networks," *IEEE J. Sel. Areas Commun.*, vol. 30, no. 3, pp. 509–524, Apr. 2012.
[47] W. M. Gifford, A. Conti, M. Chiani, and M. Z. Win, "On the SNR penalties of ideal and non-ideal subset diversity systems," *IEEE Trans. Inf. Theory*, vol. 58, no. 6, pp. 3708–3724, June 2012.
[48] H. Shin and J. H. Lee, "On the error probability of binary and M-ary signals in Nakagami-m fading channels," *IEEE Trans. Commun.*, vol. 52, no. 4, pp. 536–539, Apr. 2004.
[49] H. Shin and M. Z. Win, "MIMO diversity in the presence of double scattering," *IEEE Trans. Inf. Theory*, vol. 54, no. 7, pp. 2976–2996, July 2008.
[50] H. Shin and J. H. Lee, "Capacity of multiple-antenna fading channels: Spatial fading correlation, double scattering, and keyhole," *IEEE Trans. Inf. Theory*, vol. 49, no. 10, pp. 2636–2647, Oct. 2003.
[51] ——, "Performance analysis of space–time block codes over keyhole Nakagami-m fading channels," *IEEE Trans. Veh. Technol.*, vol. 53, no. 2, pp. 351–362, Mar. 2004.
[52] Y. Song, H. Shin, and E.-K. Hong, "MIMO cooperative diversity with scalar-gain amplify-and-forward relaying," *IEEE Trans. Commun.*, vol. 57, no. 7, pp. 1932–1938, July 2009.

Youngmin Jeong (S'09) received the B.E. and M.E. degrees in electronics and radio engineering from Kyung Hee University, Yongin, Korea, in 2009 and 2011, respectively. He is currently working toward the Ph.D. degree in electronics and radio engineering at Kyung Hee University. His current research interests include wireless communications, cooperative communications, and heterogeneous networks.

Jo Woon Chong (S'02) received the B.S. M.S., and Ph.D. degrees in electrical engineering from the Korea Advanced Institute of Science and Technology (KAIST), Daejeon, Korea, in 2002, 2004, and 2009, respectively.

In 2010, he joined the Laboratory for Information and Decision Systems (LIDS) at the Massachusetts Institute of Technology (MIT), where he is currently a Postdoctoral Fellow. From September 2009 to December 2009, he was a Postdoctoral Fellow at the Communications and Coding Theory Laboratory, Kyung Hee University, Yongin-si, Korea. His research interests include cognitive radios systems, security communication systems, game theory, cross-layer design for communication systems, resource management, multiple access technologies for WLANs and WPANs, and ultra-wideband (UWB) communication systems.

Hyundong Shin (S'01-M'04-SM'11) received the B.S. degree in electronics engineering from Kyung Hee University, Korea, in 1999, and the M.S. and Ph.D. degrees in electrical engineering from Seoul National University, Seoul, Korea, in 2001 and 2004, respectively.

From September 2004 to February 2006, Dr. Shin was a Postdoctoral Associate at the Laboratory for Information and Decision Systems (LIDS), Massachusetts Institute of Technology (MIT), Cambridge, MA, USA. In 2006, he joined Kyung Hee University, Korea, where he is now an Associate Professor at the Department of Electronics and Radio Engineering. His research interests include wireless communications and information theory with current emphasis on MIMO systems, cooperative and cognitive communications, network interference, vehicular communication networks, and intrinsically secure networks.

Professor Shin has served as a member of the Technical Program Committee (TPC) for a number of international conferences. He served as the Technical Program Co-chair for the PHY Track of the IEEE Wireless Communications and Networking Conference (WCNC) in 2009 and the Communication Theory Symposium of the IEEE Global Communications Conference (Globecom) in 2012. Dr. Shin is currently an Editor for the IEEE TRANSACTIONS ON WIRELESS COMMUNICATIONS. He was a Guest Editor for the *EURASIP Journal on Advances in Signal Processing* (Special Issue on Wireless Cooperative Networks) in 2008.

Professor Shin was honored with the Knowledge Creation Award in the field of computer science from the Korean Ministry of Education, Science and Technology in 2010. He received the IEEE Communications Society William R. Bennett Prize Paper Award (2012), Guglielmo Marconi Prize Paper Award (2008), the IEEE Vehicular Technology Conference (VTC) Best Paper Award in Spring 2008, and the IEEE VTS APWCS Best Paper Award in 2010.

Moe Z. Win (S'85-M'87-SM'97-F'04) received both the Ph.D. in electrical engineering and M.S. in applied mathematics as a Presidential Fellow at the University of Southern California (USC) in 1998. He received an M.S. in electrical engineering from USC in 1989, and a B.S. (*magna cum laude*) in electrical engineering from Texas A&M University in 1987.

He is a Professor at the Massachusetts Institute of Technology (MIT). Prior to joining MIT, he was at AT&T Research Laboratories for five years and at the Jet Propulsion Laboratory for seven years. His research encompasses fundamental theories, algorithm design, and experimentation for a broad range of real-world problems. His current research topics include network localization and navigation, network interference exploitation, intrinsic wireless secrecy, adaptive diversity techniques, and ultra-wide bandwidth systems.

Professor Win is an elected Fellow of the AAAS, the IEEE, and the IET, and was an IEEE Distinguished Lecturer. He was honored with two IEEE Technical Field Awards: the IEEE Kiyo Tomiyasu Award (2011) and the IEEE Eric E. Sumner Award (2006, jointly with R. A. Scholtz). Together with students and colleagues, his papers have received numerous awards including the IEEE Communications Society's Stephen O. Rice Prize (2012), the IEEE Aerospace and Electronic Systems Society's M. Barry Carlton Award (2011), the IEEE Communications Society's Guglielmo Marconi Prize Paper Award (2008), and the IEEE Antennas and Propagation Society's Sergei A. Schelkunoff Transactions Prize Paper Award (2003). Highlights of his international scholarly initiatives are the Copernicus Fellowship (2011), the Royal Academy of Engineering Distinguished Visiting Fellowship (2009), and the Fulbright Fellowship (2004). Other recognitions include the Laurea Honoris Causa from the University of Ferrara (2008), the Technical Recognition Award of the IEEE ComSoc Radio Communications Committee (2008), and the U.S. Presidential Early Career Award for Scientists and Engineers (2004).

Dr. Win is an elected Member-at-Large on the IEEE Communications Society Board of Governors (2011–2013). He was the chair (2004–2006) and secretary (2002–2004) for the Radio Communications Committee of the IEEE Communications Society. Over the last decade, he has organized and chaired numerous international conferences. He is currently an Editor-at-Large for IEEE WIRELESS COMMUNICATIONS LETTERS, and serves on the Editorial Advisory Board for the IEEE TRANSACTIONS ON WIRELESS COMMUNICATIONS. He served as Editor (2006–2012) for the IEEE TRANSACTIONS ON WIRELESS COMMUNICATIONS, and served as Area Editor (2003–2006) and Editor (1998–2006) for the IEEE TRANSACTIONS ON COMMUNICATIONS. He was Guest-Editor for the PROCEEDINGS OF THE IEEE (2009) and IEEE JOURNAL ON SELECTED AREAS IN COMMUNICATIONS (2002).